STUDY OF THE BEHAVIOUR OF GRANULATED BENTONITE COMPACTED AT DIFEERENT DENSITIES

A dissertation submitted in

Partial fulfillment of the requirements for the award of the degree of

MASTER OF TECHNOLOGY

In

CIVIL ENGINEERING

(With specialization in Geotechnical Engineering)

Under

ASSAM SCIENCE AND TECHNOLOGY UNIVERSITY

SESSION: 2023-2025

Submitted by:

NAMBRATA BASUMATARY

M.TECH 3rd Semester

Roll No: PG/CE/23/09

ASTU Registration No: 322208118 of 2023-2025

Under the guidance of:

DR. (MRS.) BINU SHARMA

Professor, Assam Engineering College

Department of Civil Engineering

ASSAM ENGINEERING COLLEGE

JALUKBARI, GUWAHATI-13, ASSAM

DECLARATION

I hereby declare that the work presented in this report entitled **"STUDY OF THE BEHAVIOUR OF GRANULATED BENTONITE COMPACTED AT DIFEERENT DENSITIES"** in partial fulfillment of the requirement for the award of the degree of Master of Technology in Civil Engineering with specialization in Geotechnical engineering submitted to the Department of Civil Engineering, Assam Engineering College, Jalukbari, Guwahati-13 under Assam Science and Technology University, is an authentic record of my own work carried out in the said college for six months under the supervision and guidance of Dr. Binu Sharma, Professor, Department of Civil Engineering, Assam Engineering College, Jalukbari, Guwahati13, Assam. I do hereby declare that this project report is solemnly done by me and is my effort and that no part of it has been plagiarized without citation.

Date:

Place:

Name: NAMBRATA BASUMATARY
M.Tech 3rd Semester
College Roll No: PG/C/23/09
ASTU Roll No: 230620062007
ASTU Registration No: 32228118
Department of Civil Engineering
Assam Engineering College
Jalukbari, Guwahati- 781013

CERTIFICATE OF SUPERVISION

This is to certify that the work presented in this report entitled **—** "**STUDY OF THE BEHAVIOUR OF GRANULATED BENTONITE COMPACTED AT DIFEERENT DENSITIES**" is carried out by Nambrata Basumatary, Roll No: PG/CE/23/09, a student of M.Tech 3rd semester, Department of Civil Engineering, Assam Engineering College, under my guidance and supervision and submitted in the partial fulfillment of the requirement for the award of the Degree of Master of Technology in Civil Engineering with specialization in Geotechnical Engineering under Assam Science and Technology University.

DR. (MRS.) BINU SHARMA
B.E. (Gau), M.E. (U.O.R), Ph.D. (Gau)
Professor, Department of Civil Engineering,
Assam Engineering College,
Jalukbari, Guwahati-781013

CERTIFICATE FROM THE HEAD OF THE DEPARTMENT

This is to certify that the following student of M.Tech 3rd semester of Civil Engineering Department (Geotechnical Engineering), Assam Engineering College, has submitted her project on — "**STUDY OF THE BEHAVIOUR OF GRANULATED BENTONITE COMPACTED AT DIFEERENT DENSITIES**" in partial fulfillment of the requirement for the award of the Degree of Master of Technology in Civil Engineering with specialization in Geotechnical Engineering under Assam Science and Technology University.

Name: NAMBRATA BASUMATARY

College Roll No: PG/C/23/09

ASTU Roll No:

ASTU Registration No: 322208118

Date:

Place:

DR.JAYANTA PATHAK

Professor & Head of Department

Department of Civil Engineering

Assam Engineering College

Jalukbari, Guwahati- 781013

ACKNOWLEDGEMENT

I would like to express my sincere gratitude to my supervisor Dr. (Mrs.) Binu Sharma, Professor, Department of Civil Engineering, Assam Engineering College, and senior Mr. Bhaskar Jyoti Medhi, for their continuous support and encouragement throughout this project. I am deeply grateful for their invaluable supervision, constructive feedback, and the essential information they provided, which greatly contributed to the successful completion of this work. Working under their guidance has been an inspiring and rewarding experience. I express my gratitude to Dr. Jayanta Pathak, Professor and Head of the Department of Civil Engineering, Assam Engineering College, as well as to the entire faculty and staff of the Department of Civil Engineering. I am also deeply thankful to Assam Engineering College for providing the necessary infrastructure and support throughout the course, with special appreciation for the resources and facilities that greatly contributed to the successful completion of my project.

ABSTRACT

Granulated bentonite, widely used in geotechnical and environmental engineering, is a crucial material for applications such as landfill liners and hydraulic barriers due to its exceptional swelling capacity, low permeability, and mechanical stability. This study explores the behavior of granulated bentonite, specifically looking at its swelling, consolidation, and permeability properties when compacted to different densities. Laboratory experiments following Indian Standard guidelines investigated how varying dry densities affect its swelling, consolidation, and permeability behaviors when saturated with distilled water. Higher densities were found to enhance mechanical strength and reduce permeability, making them suitable for barriers, though they limit swelling capacity. Additionally, the consolidation behavior showed a semi-logarithmic relationship between void ratio and effective stress, with denser samples demonstrating lower compression indices and slower pore water dissipation. These findings highlight the importance of optimizing compaction density in the design of barrier systems, balancing both swelling pressure and permeability. The insights gained from this study are valuable for designing high-performance liner systems in geotechnical and environmental engineering, ensuring more reliable and sustainable containment solutions.

Keywords: Granulated Bentonite, Swelling Pressure, Consolidation, Permeability.

Table of Contents

List of Figures

List of Tables

CHAPTER 1
INTRODUCTION

1.1 General

Geosynthetic Clay Liners (GCLs) are advanced sealing materials extensively utilized in the geoenvironmental industry for a wide range of applications, including landfill caps and base liners, secondary containment for fuel storage facilities, and various water containment structures such as dams, canals, rivers, and lakes. It is a durable and impermeable barrier consisting of a layer of high-swelling sodium bentonite encapsulated between two geotextiles, which are mechanically bonded. The inclusion of sodium bentonite, a clay mineral primarily composed of montmorillonite, is pivotal due to its exceptional swelling capacity and low permeability. When hydrated, bentonite can swell approximately up to 900% by volume or 700% by weight, forming a highly effective seal equivalent to several feet of compacted clay. This makes GCLs a superior alternative to traditional compacted clay liners, offering technical and economic advantages such as lower hydraulic conductivity, reduced installation time, and enhanced resilience to freeze-thaw and wet-dry cycles. GCLs have demonstrated their reliability in various environmental applications, offering an efficient solution for protecting groundwater and mitigating the migration of fluids and chemicals (Herlin and Maubeuge, 2002).

Compacted bentonite is considered an ideal buffer and backfill material in high-level radioactive waste disposal repositories due to its low permeability, high swelling properties, and strong adsorption capacity. Achieving high density in bentonite powder through increased compaction energy alone is challenging. The compactness of bentonite can be significantly enhanced by modifying its grain size distribution. Granulation improves the materials behaviour by altering its grain size distribution, leading to enhanced compactness and reduced void ratios. This results in significant energy savings during compaction while maintaining comparable hydromechanical properties, such as swelling behavior, water retention capacity, and permeability, between granular and powdered forms. Granular bentonite is preferred over its powdered form due to its superior compactness achieved with less energy, simplified handling, and better mechanical stability. These advantages make granular bentonite particularly suitable for critical applications, such as high-level radioactive waste repositories, where compactness and efficiency are paramount (Tan et al., 2020).

The density of granulated bentonite also has a profound impact on its properties and performance across various applications. Higher density reduces permeability by compacting particles and minimizing void spaces, making it a more effective barrier against water and contaminants. It also enhances mechanical strength and thermal conductivity, both of which are crucial for stability and durability. However, higher density limits the swelling capacity of bentonite, as compacted particles have less space to expand. Conversely, lower density allows for greater swelling and improved cation exchange capacity (CEC) but compromises mechanical strength, permeability, and thermal conductivity due to increased void spaces. These effects make high-density bentonite ideal for applications such as sealing barriers and landfill liners, where low permeability and mechanical stability are critical. On the other hand, lower-density bentonite is more suitable for applications like drilling muds, which prioritize fluidity and swelling. (Nazir et.al, 2021)

1.2 Objectives of the Study

The objectives of this study are as follows:

- To study the oedometric swelling and swelling pressure of granulated bentonite of different densities when permeated with distilled water.
- To study consolidation characteristics of granulated bentonite of different densities when permeated with distilled water.
- To study permeability characteristics of granulated bentonite of different densities when permeated with distilled water.

CHAPTER 2

Background and Literature Review

2.1 General

Granulated bentonite is a material of significant interest in geotechnical and environmental engineering due to its ability to swell and seal, making it essential for applications such as landfill liners and hydraulic barriers. The behavior of bentonite, especially when compacted at different densities, plays a critical role in its effectiveness for such applications. This literature review examines the behavior of granulated bentonite under varying compaction densities, focusing on its swelling behavior, swelling pressure, compression characteristics, consolidation properties, and permeability. By analyzing the effects of different densities on these key characteristics, this review aims to provide a comprehensive understanding of how compaction influences bentonite performance. The review is organized to explore the effect of compaction densities on these properties, highlighting key trends and challenges that may influence future studies and applications.

2.2 Literature Review

This report presents a review of key papers and studies in this field. The main findings and contributions from various research sources are given below.

Baille et al. (2010) studied the swelling pressures and one-dimensional compressibility behavior of compacted bentonite under controlled laboratory conditions. They used a high-pressure oedometer to assess the effects of varying initial dry densities and water contents on bentonite behavior during saturation and subsequent consolidation up to 25 MPa. A key finding was that swelling pressures increase with higher dry densities but decrease with higher initial water contents due to changes in the clay fabric. Compression behavior also varied, with compacted specimens demonstrating distinct compression paths compared to initially saturated specimens, which maintained larger void ratios at equivalent pressures. It was also found that at very high pressures, the differences in fabric between initially saturated and compacted saturated specimens diminished, leading to similar compressibility behavior. However, compacted specimens exhibited higher permeability and lower compression indices than initially saturated specimens, reinforcing the influence of compaction conditions on structural characteristics.

Additionally, the void ratio-permeability relationship for compacted specimens was linear, in contrast to the bilinear trend observed for initially saturated specimens.

Cantillo et al. (2017) developed empirical correlations to estimate the swelling pressure of expansive clays in Barranquilla, Colombia, by analyzing the influence of key soil properties such as water content and Atterberg limits. Their findings reveal that swelling pressure decreases significantly with increasing water content, highlighting the critical role of moisture in expansive soil behavior. Atterberg limits were determined to be statistically insignificant for predicting swelling pressure in the studied soils. The study employed standardized laboratory methods, including the constant volume technique, to generate reliable data for developing predictive models. These correlations are specific to the mineralogical and geotechnical characteristics of the tested clays, limiting their applicability to other regions.

Domitrović and Kovačević Zelić (2013) conducted a study to examine the relationship between swelling behavior and shear strength properties of bentonite, focusing on granular Volclay bentonite, predominantly composed of montmorillonite (80–85%). The study has found that the primary stage swelling was completed after 31 days regardless of the normal stress intensity. After primary swelling the stage of secondary compression and creep develops. The extent of swelling and secondary compression depends on the normal stress levels. Shear strength analysis showed that cohesion decreases with extended hydration, with significant changes in the first 14 days. The friction angle increases when hydrated up to 14 days but stabilizes with further hydration.

Wang (2024) advanced the measurement techniques for apparent swelling pressure in compacted bentonite by addressing the limitations of conventional methods that use 10–20 mm thick specimens, which require weeks or months of testing due to bentonites low hydraulic conductivity. While earlier attempts to reduce specimen thickness to 2 mm improved efficiency, challenges in accuracy persisted. Wang introduced a novel apparatus for testing 0.4 mm thick specimens, reducing the testing time to 1–2 hours. The study confirmed that thinner specimens retained the swelling pressure evolution trends observed in thicker ones, including an initial peak, reduction due to particle rearrangement, and eventual equilibrium. Despite minor data scatter from variations in montmorillonite content and dry density measurements, the results were consistent with previous findings, validating the reliability of the new method.

Jeon and Lyoo (2009) investigated the swelling properties of sodium bentonites under various chemical and physical conditions, emphasizing the impact of ion valence, cation size, temperature, and pH. The study found that swelling behavior varies significantly with the type of cation present, with mono-valent ions like Na+ and K+ promoting higher swelling compared to bi-valent ions such as Ca2+ and Mg2+. Experiments conducted with solutions like NaCl, KCl, CaCl2, and MgCl2 between temperature ranges of 16°C to 60°C revealed that higher temperatures accelerate swelling stabilization, with powder forms of bentonite stabilizing faster than granular forms. Then extreme pH levels, whether acidic or alkaline, were found to notably affect swelling properties.

Liu et al. (2011) examined the permeability and swelling behavior of natural bentonite MX-80 in distilled water, focusing on its unique characteristics compared to purified Na-exchanged bentonite due to the presence of approximately 20% accessory minerals. These minerals play a significant role in influencing MX-80's swelling and hydraulic properties, resulting in a slower expansion process and forming a three-component system. The study utilized a dynamic force balance model, originally designed for Na-bentonite, and a Kozeny–Carman-like (KC-like) equation to predict MX-80's swelling behavior. By applying a "lumped" approach that treats accessory minerals as part of the solid structure and a "stepwise" approach to account for gradual changes in pore water chemistry, the model successfully replicated experimental results. The authors concluded that the KC-like equation effectively describes MX-80's permeability in dilute solutions, while the force balance model, with minor modifications, captures its swelling behavior.

Lu et al. (2023) investigated the anisotropic swelling pressure of compacted GMZ bentonite to enhance its application in high-level radioactive waste disposal systems. The study used specially developed apparatuses to evaluate swelling pressure in three orthogonal directions and explored factors such as initial suction, dry density, and specimen preparation methods. It was found that the swelling pressure parallel to the compaction axis consistently exceeded that in perpendicular directions, with anisotropy decreasing during hydration. The swelling pressure increased significantly with higher dry density, showing a 9.6-fold rise as dry density increased from 1.5 to 1.9 Mg/m^3. The specimens with greater initial suction exhibited faster swelling rates and more pronounced intermediate phases.

Mollins et al. (1996) conducted a study to predict the properties of bentonite-sand mixtures. The research involved one-dimensional swelling and hydraulic conductivity tests on mixtures of Na-bentonite powder and sand, with bentonite contents of 5%, 10%, and 20% by weight, under vertical effective stresses of up to 450 kPa. The findings indicated that Na-bentonite powder exhibited a linear relationship between void ratio and the logarithm of vertical effective stress, regardless of the preparation method. However, sand-bentonite mixtures deviated from this behavior beyond a specific threshold stress, which depended on the bentonite content. Additionally, a near-linear relationship was identified between the logarithm of hydraulic conductivity and void ratio, offering a predictive framework for hydraulic properties.

Nagaraj et al. (2013) investigated the swelling behavior of expansive soils, emphasizing the influence of vertical drains and initial dry densities. Their study demonstrated that the introduction of vertical drains significantly increased both the percent swell and swelling pressure while reducing moisture content variation across the sample. Vertical drains notably reduced the time required for initial and primary swelling by nearly 50% and enhanced water access within the soil, leading to improved swelling behavior. The researchers successfully applied the rectangular hyperbola concept to predict ultimate swell and swelling pressure, enabling early termination of tests without waiting for equilibrium conditions. While the presence of vertical drains had minimal impact on the rate of secondary swelling and the consolidation behavior, the pre-consolidation pressure was found to increase with density and decrease with the number of drains due to enhanced water accessibility. The findings underline the effectiveness of vertical drains in improving testing accuracy and efficiency, offering practical solutions for managing the behavior of expansive soils in engineering applications.

Nazir et al. (2021) investigated the properties and applications of granulated bentonite mixtures (which consist of granules (highly compressed pellets) and powders in a mix of graded proportions) for engineered barrier systems in radioactive waste disposal. The study highlighted advantages of granulated bentonite mixtures over compacted bentonite blocks, such as easier handling during emplacement, better compaction properties, and flexibility in adapting to uneven rock surfaces. It was found that the dry density of granulated bentonite mixtures depends on particle size distribution, compaction methods, and the amount of fine particles. The study found that thermal conductivity improves when dry density and moisture content increase. Hydraulic

properties, such as water retention and conductivity depend on dry density and salinity. Higher dry density also improves mechanical properties like swelling pressure.

Pusch (1980) conducted a comprehensive study on the swelling pressure of highly compacted bentonite**.** The study explored the influence of bulk density, ion exchange, and temperature on swelling pressure. Custom-designed oedometers were used. Compacting bentonite powders with controlled water content, followed by hydration with distilled water, artificial groundwater (Allard water), and salt solutions (NaCl and $CaCl_2$) were used. Tests was performed at room temperature (20°C) and elevated temperatures (up to 90°C) which revealed a significant dependence of swelling pressure on bulk density and temperature. At densities above 2.05 t/m^3**,** swelling pressure exhibited minimal sensitivity to pore water chemistry. Lower densities were more influenced by ionic composition. Elevated temperatures reduced swelling pressures by up to 50%, attributed to weakened interlayer water structures and increased particle mobility. The study further demonstrated time-dependent evolution of bentonite homogeneity, with equilibrium conditions requiring weeks to months at ambient temperatures but occurring faster under higher thermal conditions.

Shirazi et al. (2010) investigated the permeability and swelling characteristics of bentonite and bentonite-sand mixtures. Using falling head permeability tests, consolidation theory, and swelling pressure test under various conditions, it was found that higher bentonite content reduces permeability and enhances swelling pressure, making it an effective buffer material. Factors like void ratio and particle arrangement, along with temperature, were found to influence swelling behavior, with swelling pressure increasing at higher temperatures. Sodium-based bentonites, such as Superclay and Kunigel, showed superior swelling characteristics compared to calcium-based Akagibentonite due to their higher montmorillonite content.

Sivapullaiah et al. (1996) studied the swelling behavior of bentonite clay mixed with non-swelling coarser fractions of varying sizes and shapes. Observations reveal that swelling occurs in three distinct stages: intervoid swelling, primary swelling and secondary swelling. Intervoid swelling, which takes place within the voids formed by the coarser non swelling particles, is significant when the size and proportion of the non-swelling fraction are large, though it does not contribute to the overall volume increase. Primary swelling, constituting approximately 80% of the total swelling, follows a rectangular hyperbolic relationship with time and is more immediate in mixtures with smaller non swelling fractions but delayed in mixtures with larger and coarser

particles. Secondary swelling, a slower and continuous process that follows primary swelling, exhibits a linear relationship with logarithmic time. The study highlights that total swell per gram of clay decreases with an increase in the size of the non-swelling fraction and a decrease in swelling clay content, indicating that the total swell is not directly proportional to the percentage of expansive clay. Moreover, the minimum test time required to predict maximum swelling increases for mixtures containing larger non swelling particles.

Sridharan and Gurtug (2004) investigated the swelling behavior of compacted fine-grained soils, focusing on the effects of compaction energy. Using soils with varying plasticity, including kaolinite and montmorillonitic clay, they observed that both swelling pressure and percent swell increased significantly with compaction energy, following a linear relationship. The study identified three distinct swelling phases—initial, primary, and secondary—with secondary swelling showing a linear relationship with log time and being more pronounced in highly plastic soils. The rectangular hyperbolic relationship of time vs. percent swell allowed predictions of ultimate swelling from initial measurements. A unique relationship between swelling pressure and percent swell, independent of soil type or compaction energy was observed.

Sridharan et al. (1986) studied the swelling behavior of clays using three methods: the conventional consolidation procedure, equilibrium void ratio method, and constant volume method. The results show that the conventional method yields the highest swelling pressures, the equilibrium void ratio method provides the lowest, and the constant volume method produces intermediate values. The study identifies initial dry density as the key factor influencing swelling pressure, with moisture content having a minimal impact, aligning with osmotic pressure theory. The authors also demonstrate that swelling behavior over time can be effectively modeled using a rectangular hyperbolic relationship, offering practical predictions for ultimate swelling and pressures. This research underscores the variability in results across methods and the critical role of initial conditions and stress paths in understanding clay swelling behavior.

Watanabe and Tanaka (2021) investigate the swelling pressure and deformation behavior of compacted Na-bentonite under constrained conditions, particularly focusing on materials with slight deformability such as rocks. The research highlights that the swelling pressure decreases with increasing deformability of the constraining material. This was attributed to slight specimen deformation during hydration. The findings showed that for compacted bentonite with no consolidation history, the stress path during unloading follows the normal consolidation line

(NCL) with minor non-linear deviations in highly compacted specimens. Using the Mohr–Coulomb yield criterion, the study revealed that shear strain during saturation and one-dimensional swelling deformation leads to isotropic swelling pressure and non-linearity in unloading behavior. The authors conclude that the deformability of surrounding materials significantly affects the measured swelling pressure, especially at higher dry densities. These findings offer critical insights into designing engineered barriers, particularly for radioactive waste containment, where an understanding bentonite–rock interaction is essential.

Zeng et al. (2022) examined the influence of water chemistry on the hydro-mechanical behavior of compacted mixtures of claystone and bentonite, using MX80 (Na-bentonite) and Sardinia (Ca-bentonite) in the context of sealing materials for deep geological repositories. Their results showed that the swelling pressure of MX80 bentonite decreased significantly when hydrated with synthetic site and cement solutions, due to cation exchange transforming Na-montmorillonite into multi-cation montmorillonite. Cement solution further reduced swelling by dissolving montmorillonite and forming secondary minerals with lower swelling capacity. Sardinia bentonite, being predominantly Ca-montmorillonite, exhibited minimal cation exchange but still showed reduced swelling pressure due to osmotic effects. The study also found that both synthetic site and cement solutions increased hydraulic conductivity by enlarging large-pore volumes and reducing diffuse double-layer thickness, with these effects being more pronounced at lower dry densities. The researchers concluded that water chemistry, particularly the presence of cations and hydroxide, significantly impacts the swelling capacity and hydraulic conductivity of these mixtures, with low-density specimens being more vulnerable to such changes.

Zeng et al. (2023) investigated the swelling behavior of MX80 bentonite and Callovo-Oxfordian (COx) claystone mixtures, which are used as sealing materials in geological radioactive waste disposal. Using constant-volume swelling pressure tests and mercury intrusion porosimetry (MIP), a linear relationship between swelling pressure and dry density was found ,with higher bentonite fractions resulting in greater swelling pressures and it also showed that the inter-particle pore volume decreases as bentonite content and dry density increase, indicating significant microstructural adjustments. A method to calculate average inter-particle distances from pore size distributions was developed. This method reveals a semi-logarithmic relationship between swelling pressure and inter-particle distance, regardless of the bentonite fraction.

CHAPTER 3

Materials and Methodology

3.1 General

In this chapter, the materials and experimental methods used in this study are discussed. The laboratory experiments conducted to determine the engineering properties of the soil sample (granulated bentonite) and the pore fluid (distilled water) are explained in detail. Additionally, the characteristics of the materials and the steps involved in the testing process are elaborated.

3.2 Materials

The materials used are granulated bentonite and distilled water.

3.2.1 Granulated Bentonite

Granulated bentonite is a processed form of bentonite clay, primarily composed of montmorillonite, a mineral known for its high swelling capacity, low permeability, and excellent adsorption properties when hydrated. It is widely used in the construction of landfill liners, containment barriers, and other engineered systems designed to prevent contaminants from migrating into surrounding soil and groundwater. In liners, granulated bentonite is valued for its low permeability, which restricts the flow of liquids and gases, and its self-sealing properties, which enable it to fill cracks or voids under mechanical stress. Its resistance to various chemicals makes it suitable for use in landfills where hazardous substances are present. Additionally, the granulated form ensures ease of handling, uniform distribution, and effective compaction during installation. With its durability and ability to maintain performance under loading and environmental conditions, granulated bentonite is an ideal material for ensuring the integrity of liner systems in waste containment and environmental protection projects.

Figure 3.1: Granulated Bentonite

3.2.2 Pore Fluid

The pore fluid significantly impacts the performance of liner systems by influencing the hydraulic conductivity, swelling behavior, and chemical resistance of the clay used in the liner. The interaction between the pore fluid and clay particles determines the overall sealing efficiency of the liner system. Changes in the chemical composition of the pore fluid, such as pH, ionic strength, or the presence of contaminants, can alter the swelling capacity and permeability of the liner material. In this project, distilled water has been used as the pore fluid to study the behavior of the liner material under controlled conditions. Distilled water, purified through distillation to remove impurities and minerals, ensures consistent and neutral interactions with the material during testing.

Figure 3.2: Distilled Water

3.3 Experiments

3.3.1 Oedometric Swell and Swelling Pressure Test

The oedometer swell and swelling pressure test is conducted to evaluate the swelling characteristics of expansive soils under confined conditions, as per the guidelines outlined in IS 2720 Part (XLI)-1977. In this test, the sample is first saturated with a pore fluid and allowed to swell until it reaches a steady state or ceases further swelling. Subsequently, incremental loads are applied to compress the sample back to its original volume, and the pressure required to counteract the swelling and restore the sample to its initial height is recorded as the swelling pressure.

In this experiment, the consolidometer ring used has an internal height of 20 mm and a diameter of 60 mm, with the soil sample compacted to a height of 10 mm, which is half the ring's internal diameter. Dry granulated bentonite samples are prepared at varying densities of 1.2 gm/cc, 1.1 gm/cc, 1.0 gm/cc, 0.9 gm/cc, and 0.8 gm/cc, and compacted to a height of 10 mm within the ring. Saturation is carried out using distilled water under a seating load of 5 kN/m^2, and the expansion of the sample is recorded.

The procedure begins with boiling the porous stones in distilled water for at least 15 minutes. Once prepared, a porous stone is placed in the consolidometer apparatus, followed by a filter paper. The consolidometer ring containing the soil, compacted to the desired density, is then placed above the filter paper. Another layer of filter paper is placed on top of the soil sample, followed by another porous stone on top. The entire assembly is mounted onto the loading frame, ensuring that the loading cap transmits the load axially to the soil specimen.

A seating load of 5 kN/m^2 is applied to the loading hanger, and the initial dial gauge reading is recorded. Saturation is achieved by pouring distilled water into the assembly, causing the soil to swell. Dial gauge readings are taken at various time intervals until the swelling stabilizes. To determine the swelling pressure, incremental loads are gradually applied until the swollen soil sample is compressed back to its original height.

3.3.2 Consolidation Test

The consolidation tests were conducted using the same conventional one-dimensional consolidometer apparatus previously described for determining oedometric swell and swell pressures test. These tests were performed according to IS 2720 (Part XV)-1965. The consolidation tests were carried out on the same soil samples that were used for the oedometric

swelling tests. Once the soil samples had fully swollen in the oedometric swelling tests, the consolidation tests were initiated. Double incremental loading, starting from 10 kN/m² up to 640 kN/m², was applied. For each load increment, the compression dial readings were recorded until there was no further compression.

3.3.3 Permeability Test

The permeability of the soil samples which was saturated with distilled water was calculated theoretically using the coefficient of consolidation (C_v) values obtained after each stress increment, based on Equation (3.1)

$k=C_v \times m_v \times \gamma_w \ldots (3.1)$

Where k represents the coefficient of permeability,

m_v is the coefficient of volume compressibility,

γ_w is the unit weight of water.

The coefficient of consolidation (C_v) was determined using Taylor's square root of time fitting method.

Figure 3.3: Consolidation Setup

CHAPTER 4

Analysis of Swelling Behavior of Granulated Bentonite

4.1 General

Soils that undergo significant volume changes in response to moisture variations are referred to as swelling or expansive soils. These soils consist of montmorillonite clay minerals, having a unique layered structure, with an alumina sheet positioned between two silica sheets, allowing water to infiltrate and cause substantial volumetric expansion. The swelling behavior of these clays is primarily due to their surface properties, which enable water absorption. Swelling pressure is influenced by several factors, including the type and quantity of clay minerals, initial water content, dry density, pore fluid characteristics, stress history, confining pressure, and the effects of drying and wetting cycles. Further, there are various applications where clays soils have to be engineered to suit the desired properties as back-filling (buffer) materials for high-level nuclear waste (Yong et. al. 1986), and soils barrier for landfill liner, covers, and vertical barrier walls (Daniel and Wu, 1993; Alawaji, 1999). The material is often designed as soil mixtures between expansive clay and non-expansive soils requiring among others low shrinkage and swelling properties. Swell and Swelling pressure of an expansive soil is primarily dependent on the initial dry unit weight or void ratio and also on the moisture content. (Nagaraj et.al., 2013). Dry density refers to the mass of soil solids per unit volume, excluding water and voids. It is a critical parameter in determining the soil's compactness and the arrangement of its particles, which directly affects its response to water infiltration. The relationship between dry density and swelling is essential for geotechnical applications, such as landfill liners and embankments, where controlling the swelling characteristics of soils is critical.

4.2 Analysis of Oedometric Swelling and Swelling Pressure of Granulated bentonite

Laboratory experiments were conducted using a conventional one-dimensional consolidometer apparatus. The consolidometer cutter had dimensions of 20 mm in height and 60 mm in internal diameter. Dry granulated bentonite was placed in the cutter at varying densities of 1.2, 1.1, 1.0, 0.9, and 0.8 gm/cc, filling up to a height of 10 mm. The swelling tests were performed in accordance with IS 2720 Part (XLI)-1977 standards.

The setup involved assembling the consolidometer by placing filter papers at both the top and bottom of the soil specimen. Porous stones, pre-boiled for 15 to 30 minutes, were positioned

above and below the specimen. A seating load of 5 kN/m² was applied to the loading hanger, and the horizontal inclination of the setup was corrected before noting the initial reading of the dial gauge.

Saturation of the dry soil samples was achieved by introducing pore fluids, specifically distilled water. Upon saturation, the soil specimens began to swell, which was recorded through dial gauge readings taken at regular intervals until the swelling ceased. To determine the swelling pressure, incremental loads were gradually applied until the swollen soil sample returned to its original height, and the corresponding readings were recorded.

$$\text{Swelling percentage (\%)} = \frac{\Delta H \times 100}{H_0} \ldots (4.1)$$

Where $\Delta H = H_f - H_o$;

H_f = Final height after swelling after every 24 hrs.

H_o = Initial height before swelling (10 mm)

4.2.1 Effect of different densities of granulated bentonite on oedometric swelling

The relationship between time in days and swelling percentage for granulated bentonite at initial dry densities of 1.2, 1.1, 1.0, 0.9, and 0.8 g/cm³, when saturated with distilled water, were determined through experiment. The results of these experiments are presented in the plots shown in Figures 4.1 to 4.5.

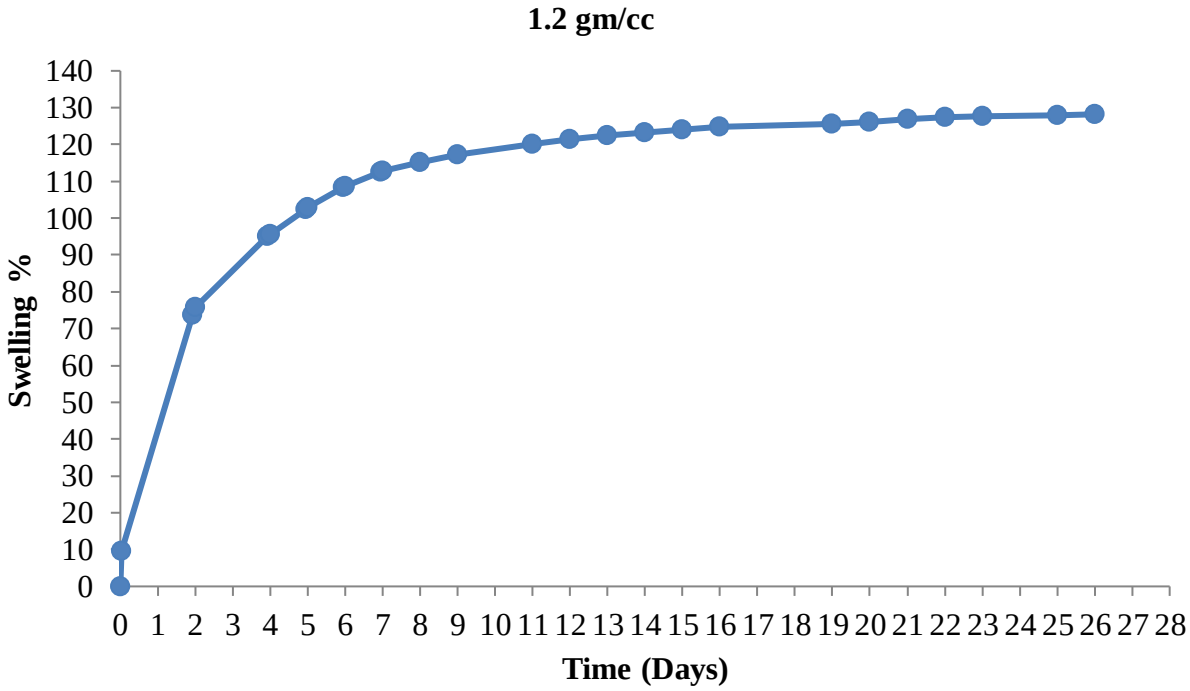

Figure 4.1: Time vs Swelling % of Granulated Bentonite at density 1.2 gm/cc

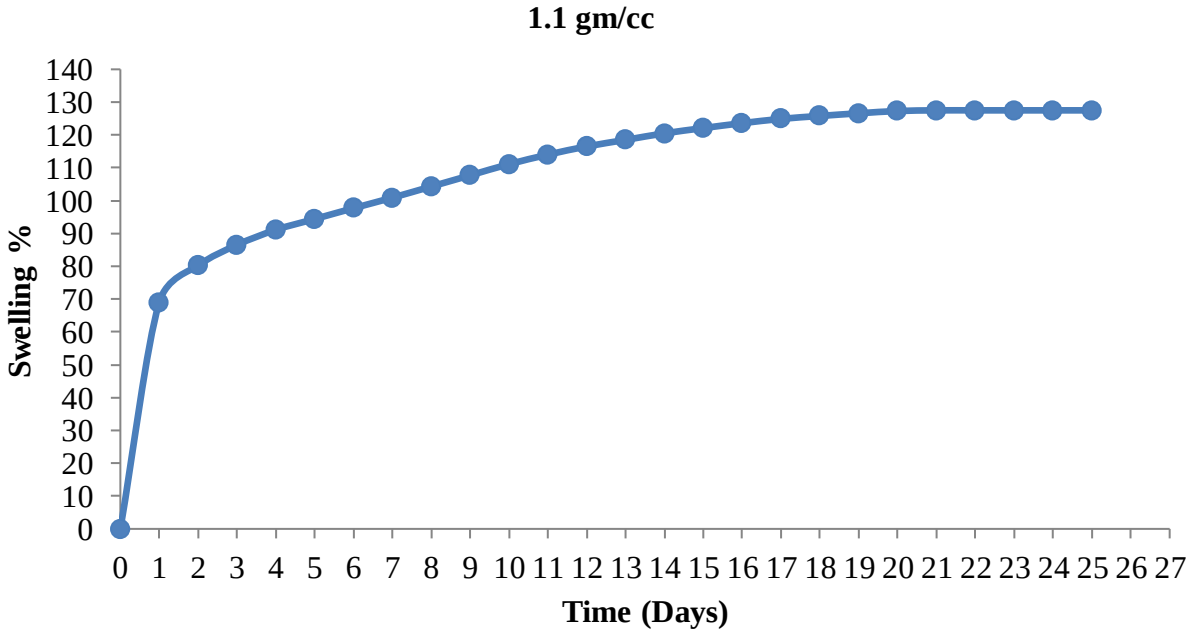

Figure 4.2: Time vs Swelling % of Granulated Bentonite at density 1.1 gm/cc

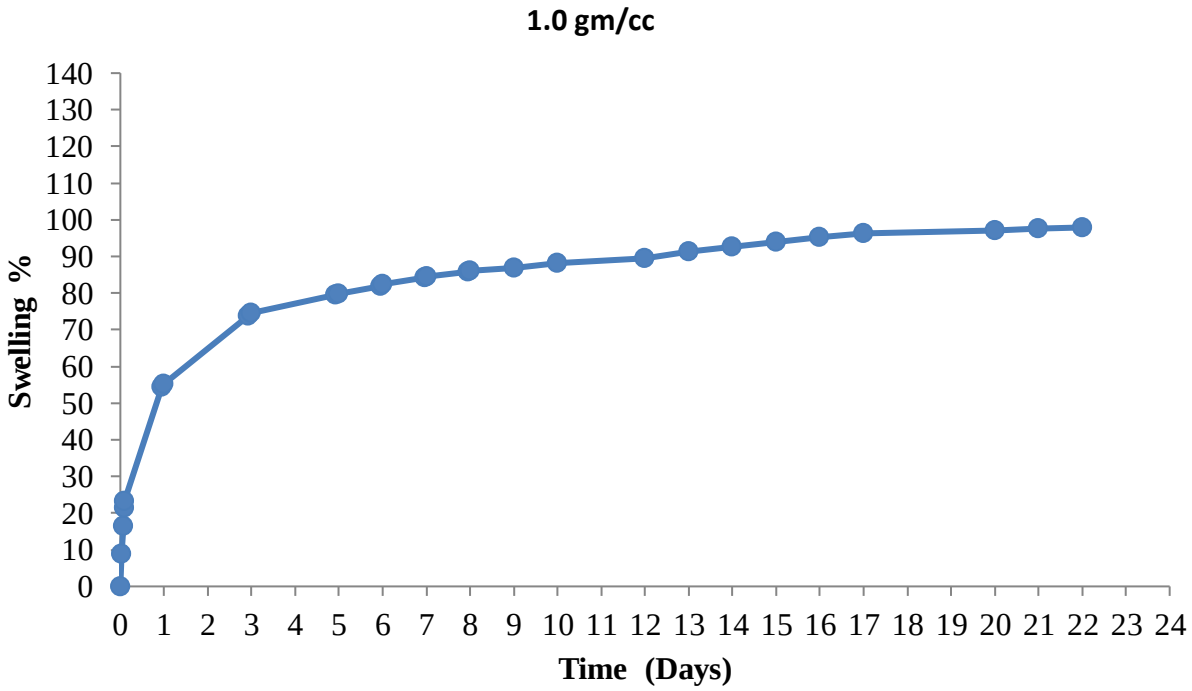

Figure 4.3: Time vs Swelling % of Granulated Bentonite at density 1.0 gm/cc

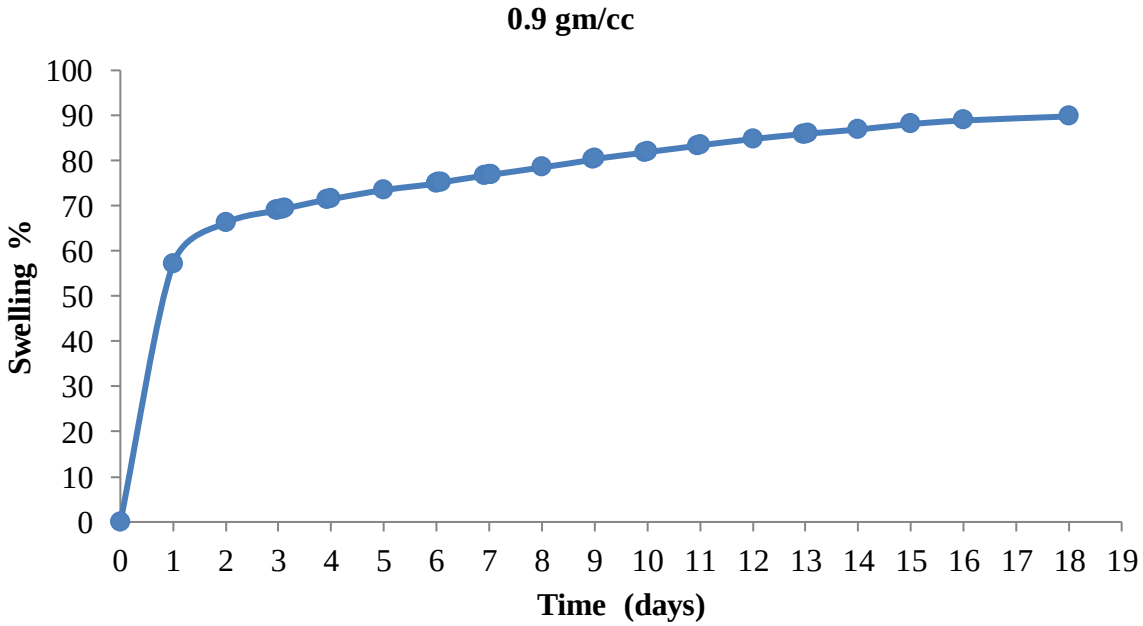

Figure 4.4 : Time vs Swelling % of Granulated Bentonite at density 0.9 gm/cc

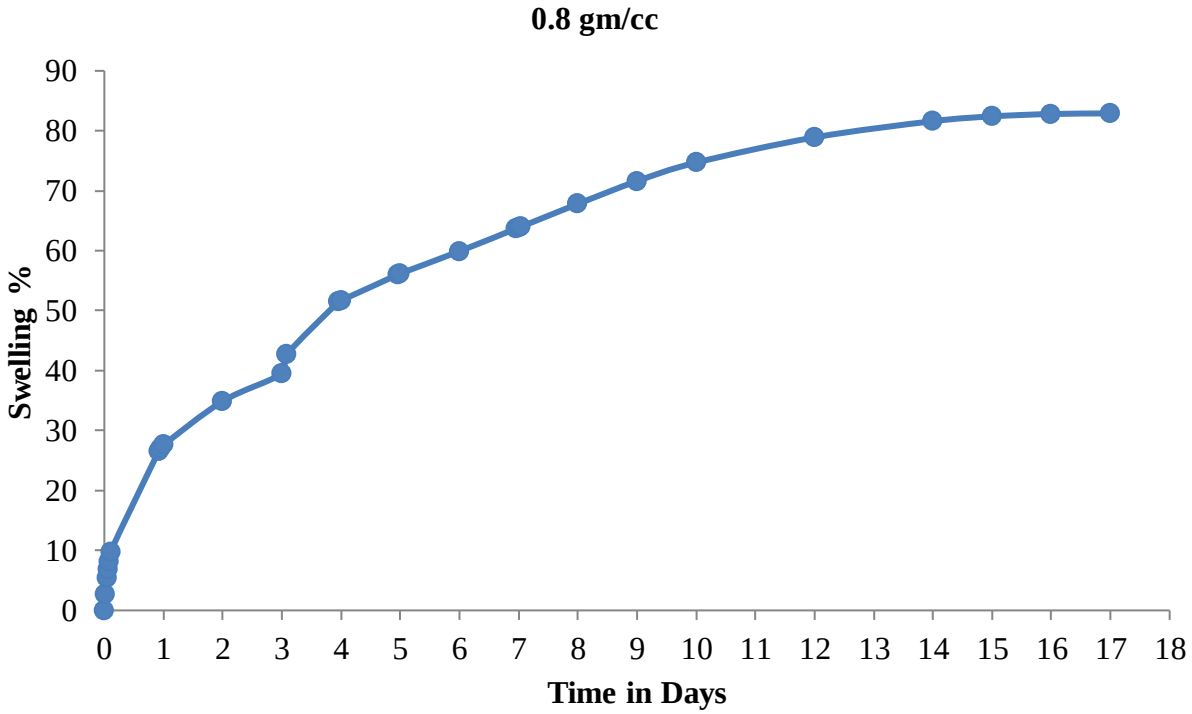

Figure 4.5: Time vs Swelling % of Granulated Bentonite at density 0.8 gm/cc

4.2.2 Comparison of the swelling curves of different densities of Granulated Bentonite

The combined graphs of swelling versus time for granulated bentonite at various densities, with distilled water as the pore fluid, are presented in Figure 4.6.

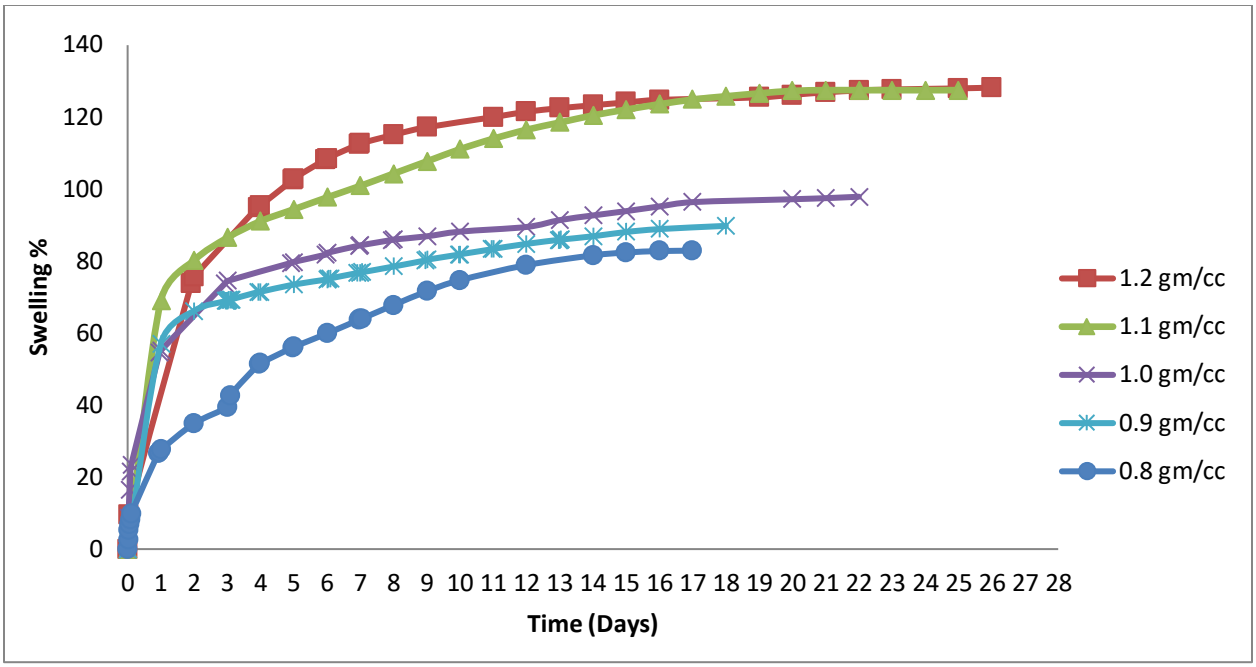

Figure 4.6: Combine graph for the Time vs. swelling % of Granulated Bentonite at different densities

The plot shows that swelling percentages generally increase over time for all densities and eventually stabilize after a certain period. The swelling percentage increases with an increase in density. Additionally, the time required for complete swelling also increases as the density increases.

4.2.3 Effect of different densities of Granulated Bentonite on Swelling Pressure

Once swelling stabilizes, the sample is gradually loaded to restore it to its original height. The load required to counteract the swelling and return the soil to its initial height is recorded as the swelling pressure. The swelling pressures for granulated bentonite were experimentally determined at dry densities of 1.2 g/cm³, 1.1 g/cm³, 1.0 g/cm³, 0.9 g/cm³, and 0.8 g/cm³ when saturated with distilled water. Table 4.1 presents the swelling pressure values for different densities, while Figure 4.7 illustrates the relationship between swelling pressure and density.

Table 4.1 : Swelling pressures of Granulated bentonite for distilled at different densities

Density (gm/cc)	Swelling Pressure (kN/m^2)
1.2	640
1.1	560
1	480
0.9	400
0.8	320

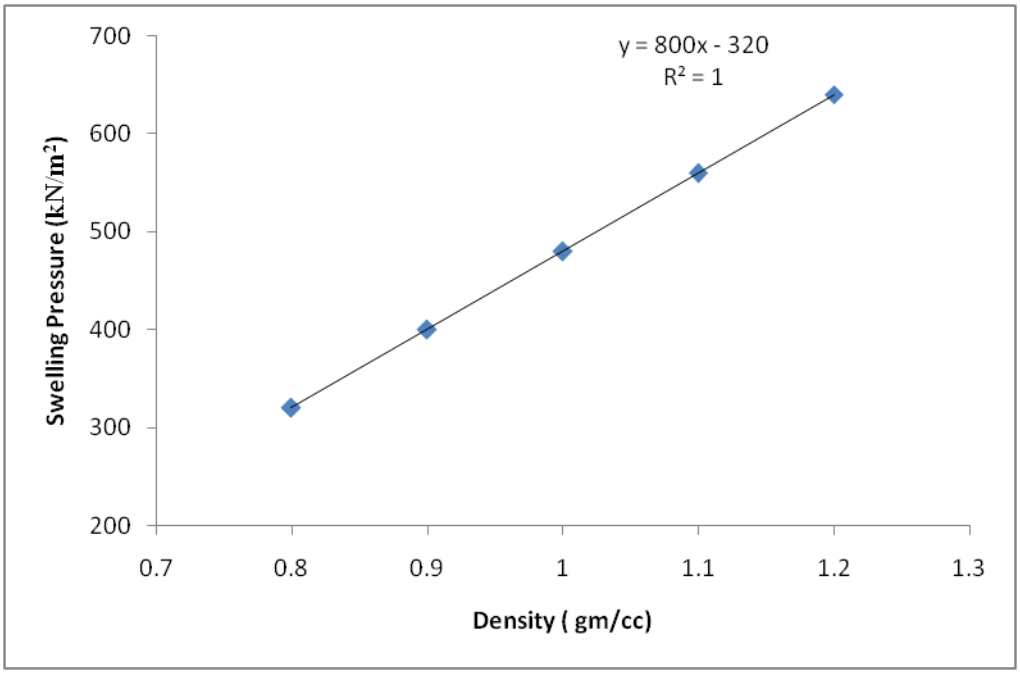

Figure 4. 7: Density vs Swelling Pressure of granulated bentonite permeated with distilled water

The plot indicates that swelling pressure generally increases with density, following a linear trend. Table 4.2 shows Swelling Percentage and Swelling Pressure at different densities

Table 4.2: Swelling Percentage and Swelling Pressure of Granulated Bentonite of Different Densities permeated with Distilled Water

Density (gm/cc)	Swelling Percentage	Swelling Pressure (kPa)
1.2	128.2	640
1.1	127.5	560
1.0	98.2	480
0.9	89.8	400
0.8	82.9	320

CHAPTER 5

Analysis of Consolidation Characteristics of Granulated Bentonite

5.1 General

When a compressive load is applied to a soil mass, a decrease in its volume occurs, which is referred to as compression, while the property of soil related to its susceptibility to decrease in volume under pressure is known as compressibility. In a saturated soil mass, where the voids are filled with incompressible water, compression takes place when water is expelled from the voids. This process, caused by long-term static loading and the subsequent escape of pore water, is termed consolidation. Consolidation tests are conducted primarily to determine the total settlement of laterally confined saturated soil under external loading and to evaluate the rate of settlement due to the gradual application of load. The total settlement is typically expressed in terms of the compression index (C_c), and the rate of settlement is defined by the coefficient of consolidation (C_v). In this chapter, the consolidation characteristics of granulated bentonite, compacted at different densities and saturated with distilled water are analyzed.

5.2 Analysis of Compressibility behaviour of Granulated bentonite at different densities

The consolidation tests commenced once the soil sample achieved full swelling during the oedometric swelling test. These tests were conducted in accordance with IS 2720 (Part XV)-1965. A double incremental loading method was employed, starting at 10 kN/m² and progressively increasing up to 640 kN/m². For each loading increment, compression dial readings were taken over a period of 48 hours, beginning at 40 kN/m². The change in void ratio corresponding to the increase in overburden pressure was calculated using the formula provided in Equation 5.1.

$$\Delta e = \frac{\Delta H\,(1+e_O)}{H} \ldots (5.1)$$

Where ΔH is the change in sample thickness due to the increase in overburden pressure

H is the initial thickness of the sample and

e_o is the initial void ratio of the sample.

Once the consolidation process is over, the sample was carefully dismantled, ensuring that no soil grains were lost, and its dry weight was recorded. Using the dry weight and the height of solids method, the void ratio was calculated. Based on the experimental studies conducted on

granulated bentonite, the variation of void ratio with effective stress was plotted graphically, as shown below from Figure 5.1 to 5.5 and combination of these graphs is shown in Figure 5.6.

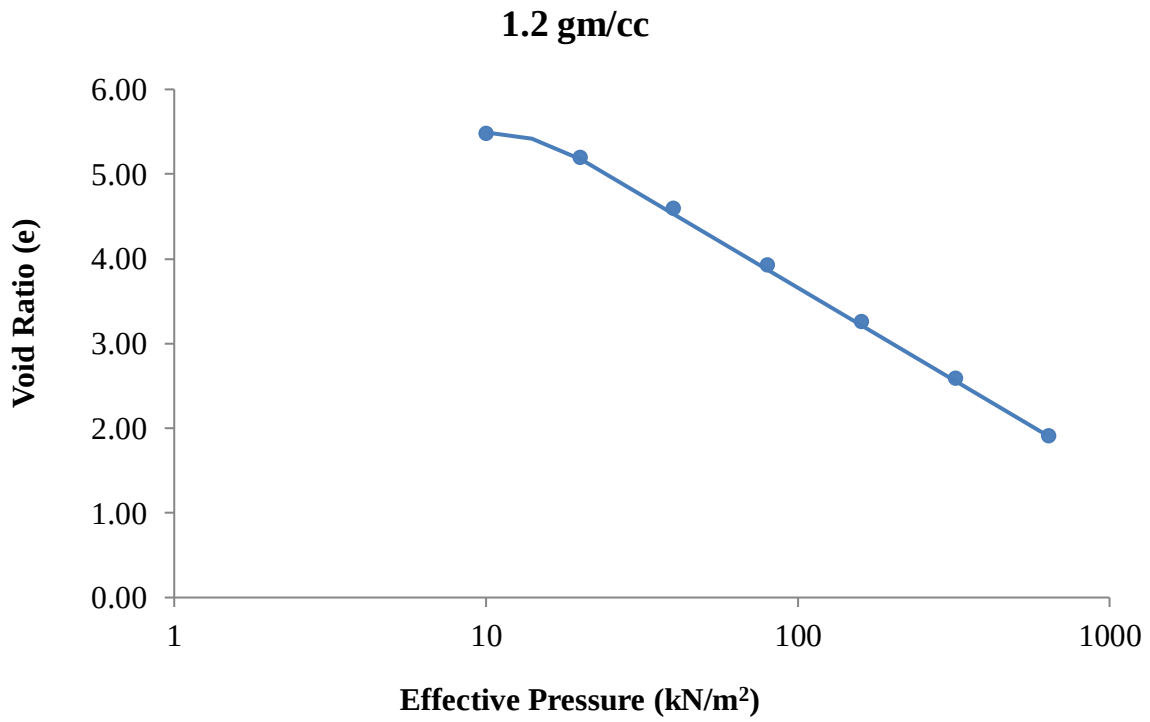

Figure 5.1: Void Ratio vs Effective Pressure of Granulated Bentonite with density 1.2 gm/cc

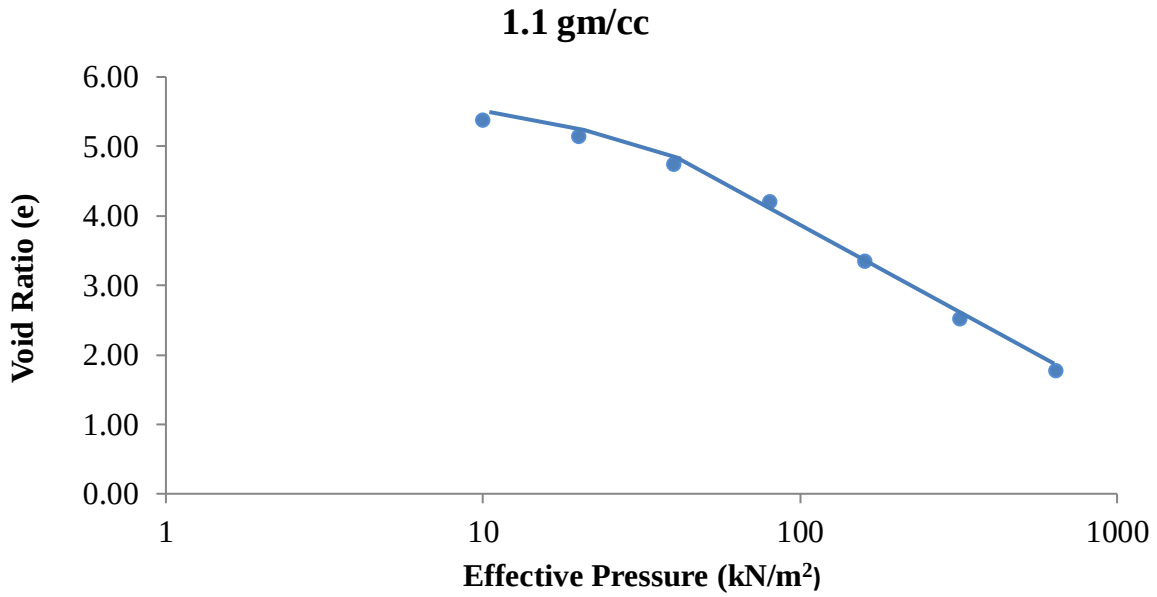

Figure 5.2: Void Ratio vs Effective Pressure of Granulated Bentonite with density 1.1 gm/cc

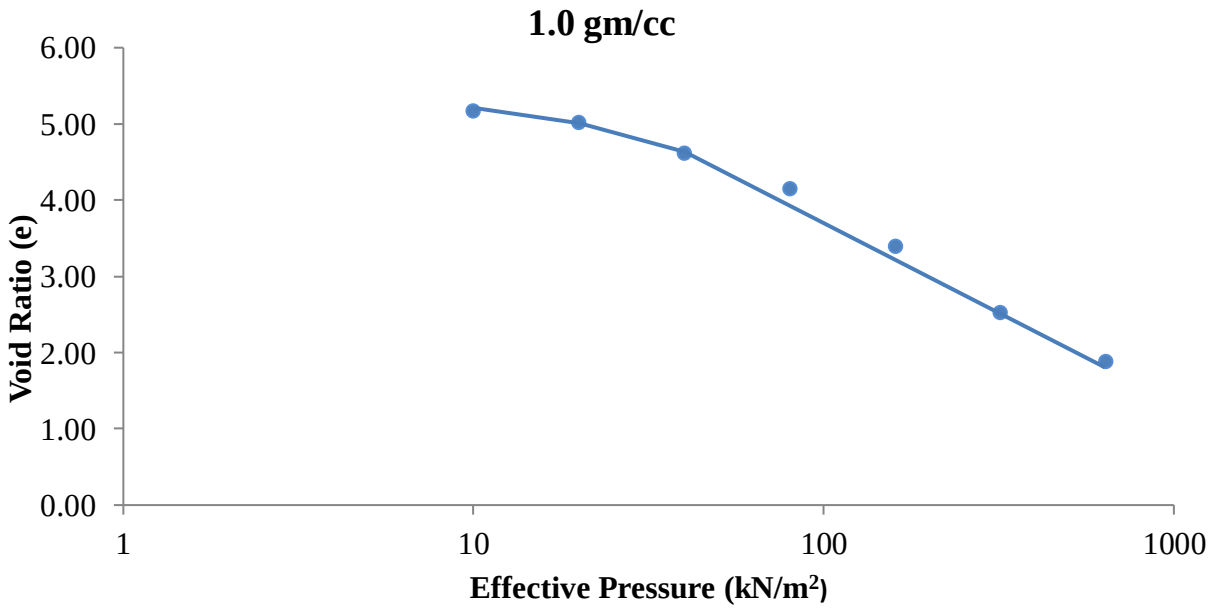

Figure 5.3: Void Ratio vs Effective Pressure of Granulated Bentonite with density 1.0 gm/cc

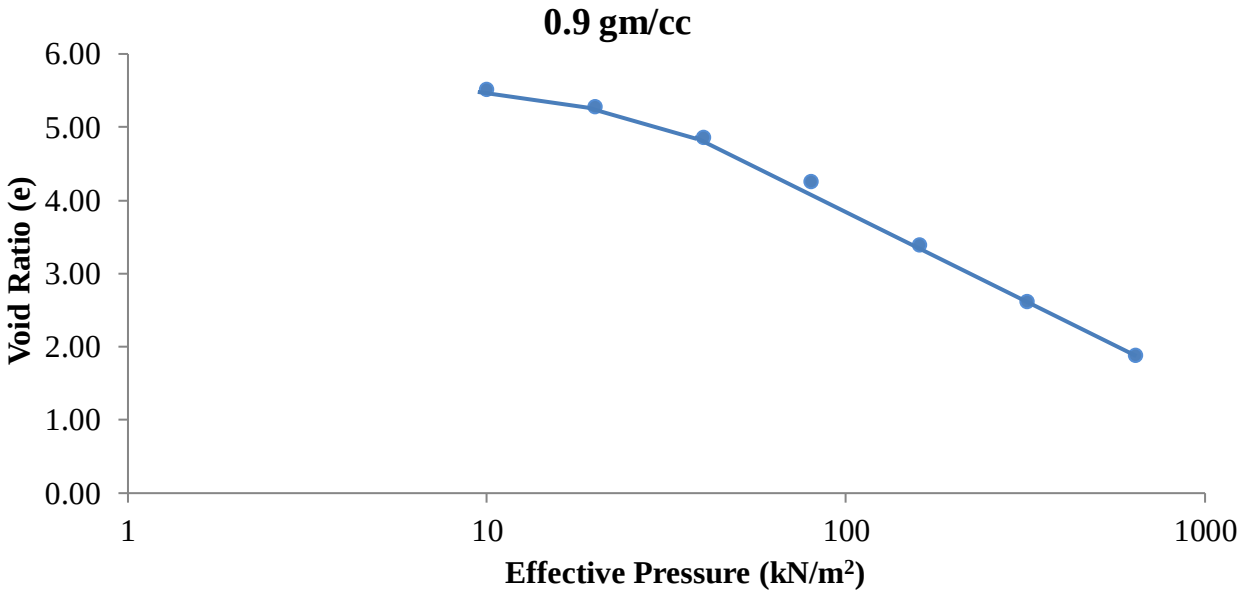

Figure 5.4: Void Ratio vs Effective Pressure of Granulated Bentonite with density 0.9gm/cc

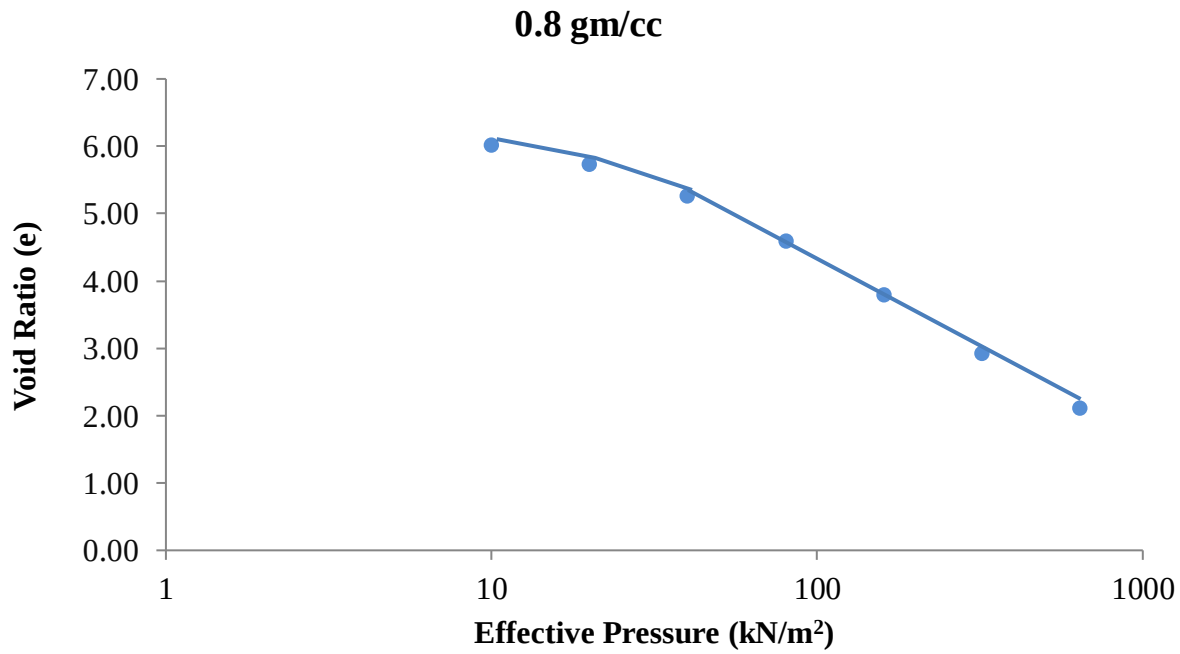

Figure 5.5: Void Ratio vs Effective Pressure of Granulated Bentonite with density 0.8 gm/cc

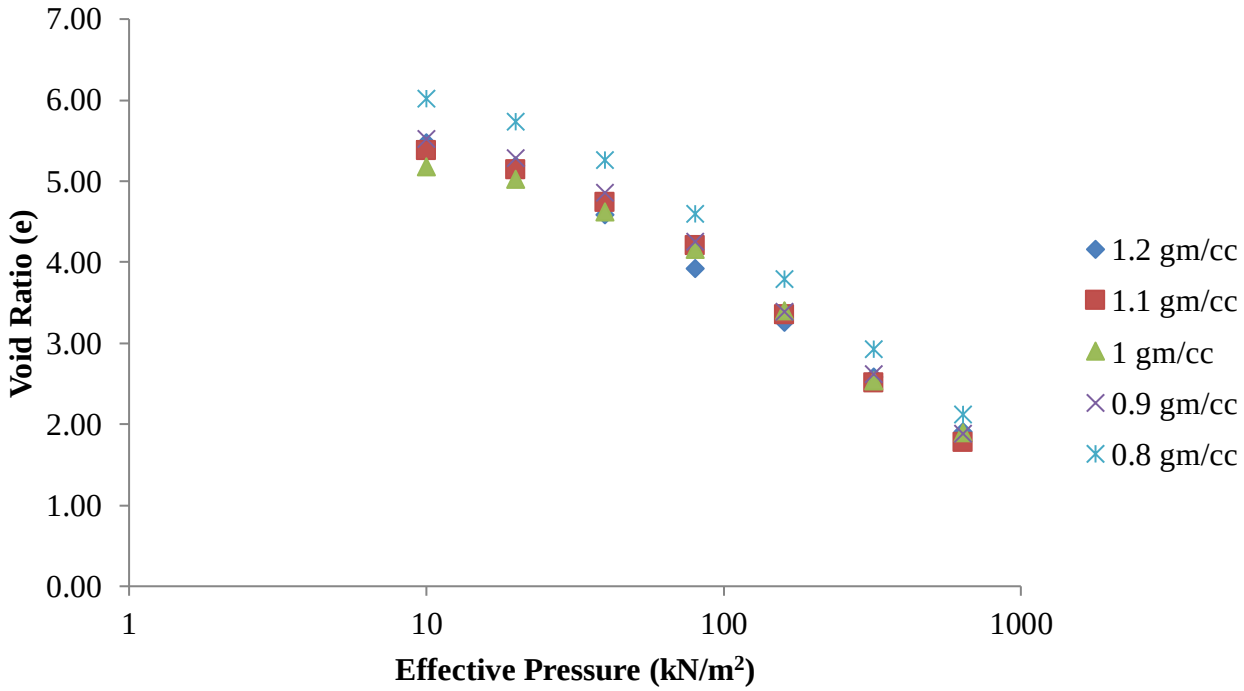

Figure 5.6: Combined graph of Void Ratio vs Effective Pressure of Granulated Bentonite at different densities

From the void ratio vs effective pressure (e vs log P) graph it had been observed that the void ratio (e) decreases with increasing effective pressure (P) for all densities, indicating a compressive behavior of soils under consolidation. Soils with higher initial densities, such as 1.2 gm/cc, exhibit lower initial void ratios and smaller reductions in void ratio under pressure, reflecting reduced compressibility. In contrast, soils with lower initial densities, like 0.8 gm/cc, have higher initial void ratios and show greater compressibility as pressure increases. At lower pressures, the differences in void ratio between densities are more pronounced, but as the pressure increases, the curves tend to converge, suggesting that compressibility differences diminish at higher pressures due to particle packing. Densely compacted samples are less compressible due to reduced void spaces, whereas loosely compacted samples are more compressible due to their higher void ratios. The semi-logarithmic trend observed in the graph aligns with typical consolidation behavior, where soils undergo a rapid reduction in void ratio at low pressures followed by a slower reduction as pressure increases.

5.3 Determination of Compression index (Cc)

The compression index (C_c) is a parameter used to quantify the compressibility of soils. It is the slope of the linear portion of the e vs log P (Void Ratio vs. Effective Pressure) curve and provides insights into the response of soil under increasing effective stress. The compression index is mathematically expressed as:

$$Cc=\frac{\Delta e}{\Delta \log P} \quad \ldots (5.2)$$

Where, Δe is the change in void ratio and

$\Delta \log P$ is the change in the logarithm of effective pressure (P).

Table 5.3: Compression Index of all the Densities

Density	Compression Index (C_c)
1.2	2.29
1.1	2.35
1.0	2.42
0.9	2.56
0.8	2.66

The table indicates an inverse relationship between density and the compression index (Cc), with higher-density samples (e.g., 1.2 gm/cc) exhibiting lower Cc values (2.29) and lower-density samples (e.g., 0.8 gm/cc) showing higher Cc values (2.66) highlighting that denser, more compacted samples are less compressible due to reduced pore spaces, while loosely compacted samples are more compressible.

5.4 Determination of Coefficient of consolidation (C_v)

The coefficient of consolidation (C_v) is a measure of the rate at which a soil undergoes consolidation when subjected to a change in load. It is used to characterize the rate at which pore water in a saturated soil is expelled as a result of an increase in applied load, leading to a reduction in volume. The coefficient is important for understanding the time-dependent settlement behavior of soils. It is determined from laboratory consolidation tests where the rate of settlement of a soil sample under a controlled loading is measured. The procedure involves

measuring the change in height of the soil sample as it is incrementally loaded. To determine the coefficient of consolidation, the change in height is plotted against the square root of time or its logarithm. In this project, the Taylor's square root of time fitting method is used to determine the coefficient of consolidation. This method involves plotting the dial gauge readings against the square root of time for each pressure increment. A straight line is drawn through the primary consolidation zone. Another straight line is drawn with a slope that is 1.15 times the slope of the previous line. This second line intersects the curve at a point, and the x-coordinate of this intersection gives the value of $\sqrt{t_{90}}$. The coefficient of consolidation 'C_v' can be calculated by the following equation:

$$C_v = \frac{T_v \times d^2}{t_{90}} \ldots (5.3)$$

Where $\sqrt{t_{90}}$ =the square root of the time taken for a soil sample to reach 90% consolidation

T_{90} = Time factor corresponding to 90% degree of consolidation = 0.848

d = Average drainage path for the pressure increment = $(H_i + H_f) / 4$

H_i = Initial height of soil

H_f = Final height obtained by height of soil method for a given pressure increment.

5.4.1 Comparison of the C_v values

The coefficient of consolidation (C_v) curves for all the samples with densities of 1.2, 1.1, 1.0, 0.9, and 0.8 gm/cc are plotted in Figures 5.7 to 5.34 respectively and the values are shown in table 5.2-5.6.

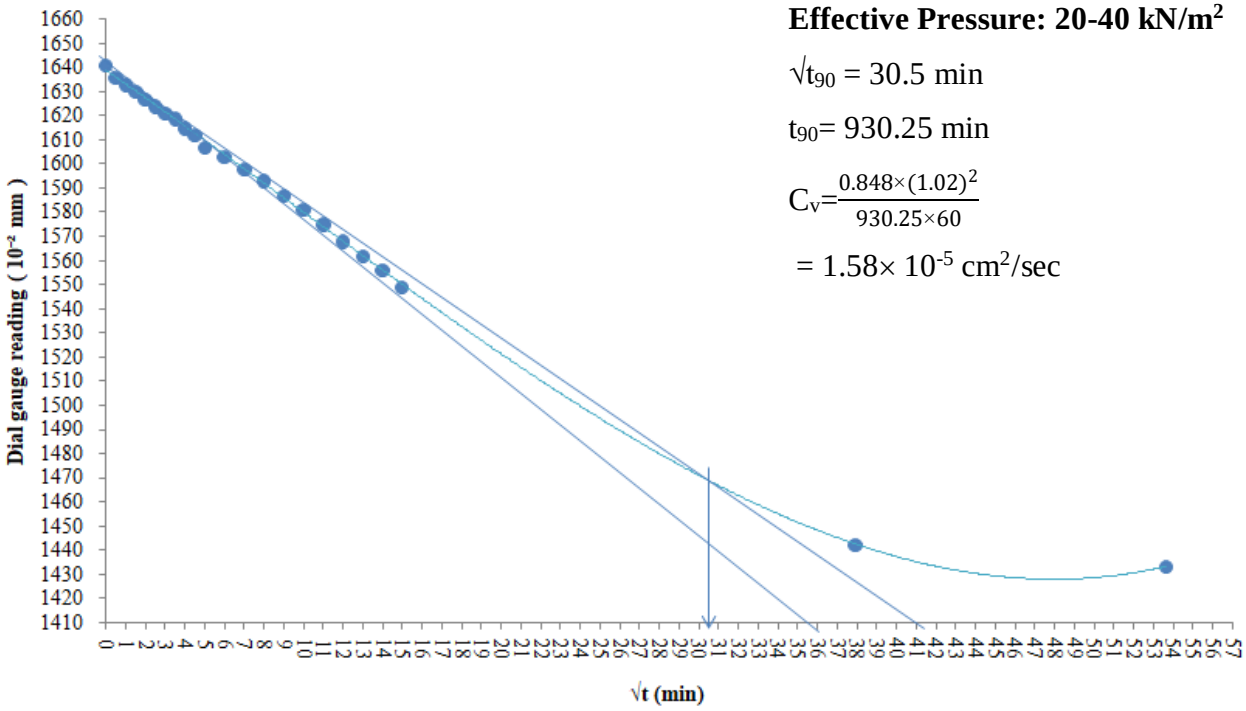

Effective Pressure: 20-40 kN/m^2

$\sqrt{t_{90}}$ = 30.5 min

t_{90}= 930.25 min

$C_v = \frac{0.848 \times (1.02)^2}{930.25 \times 60}$

= 1.58× 10^{-5} cm^2/sec

Figure 5.7: Time vs Dial Reading graph of sample with density 1.2 gm/cc at 20-40 kN/m^2

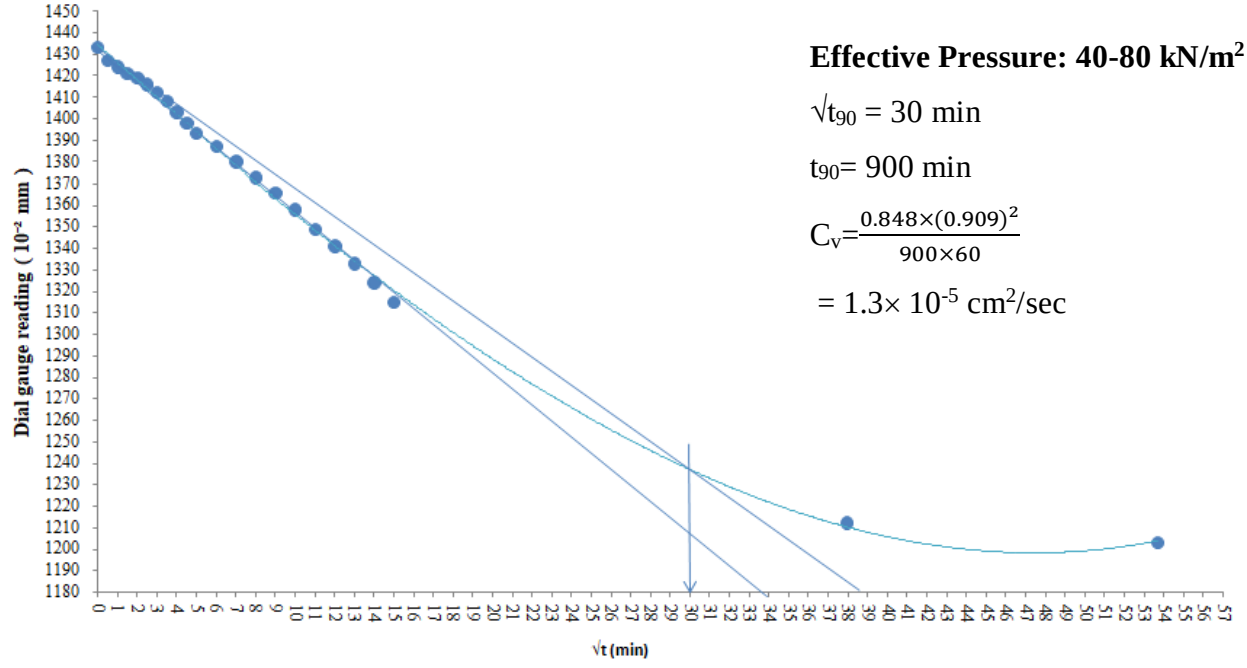

Effective Pressure: 40-80 kN/m^2

$\sqrt{t_{90}}$ = 30 min

t_{90}= 900 min

$C_v = \frac{0.848 \times (0.909)^2}{900 \times 60}$

= 1.3× 10^{-5} cm^2/sec

Figure 5.8: Time vs Dial Reading graph of sample with density 1.2 gm/cc at 40-80 kN/m^2

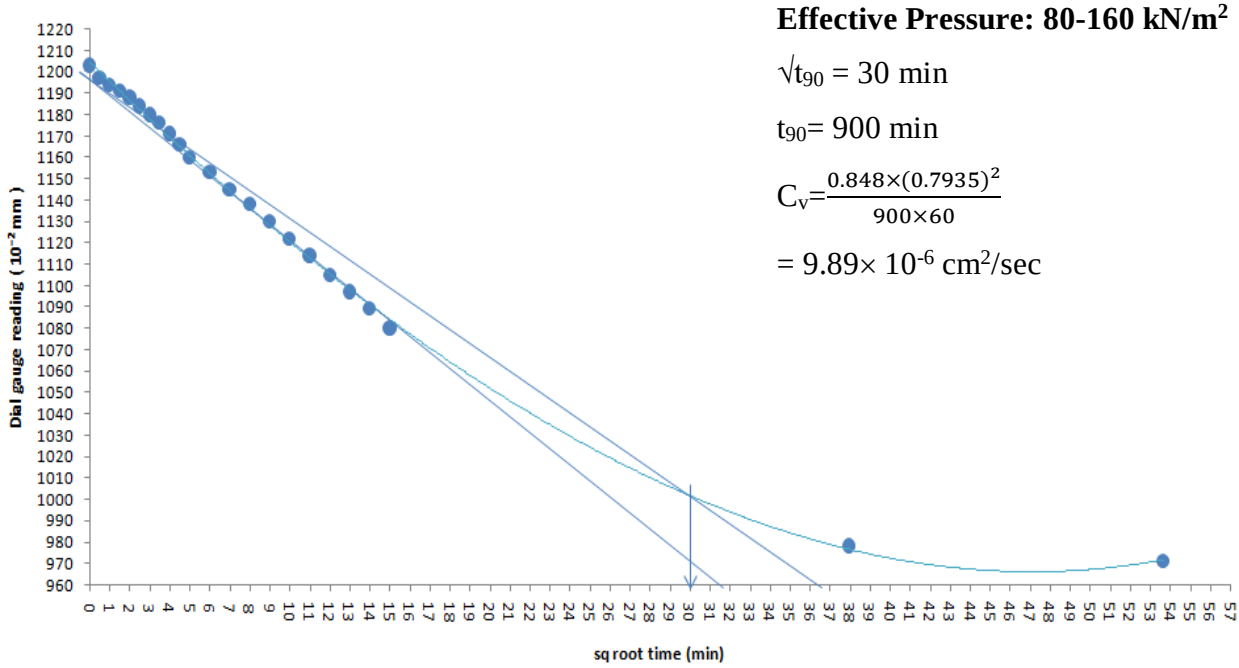

Effective Pressure: 80-160 kN/m^2

$\sqrt{t_{90}}$ = 30 min

t_{90}= 900 min

$C_v = \frac{0.848 \times (0.7935)^2}{900 \times 60}$

= 9.89× 10^{-6} cm^2/sec

Figure 5.9: Time vs Dial Reading graph of sample with density 1.2 gm/cc at 80-160 kN/m^2

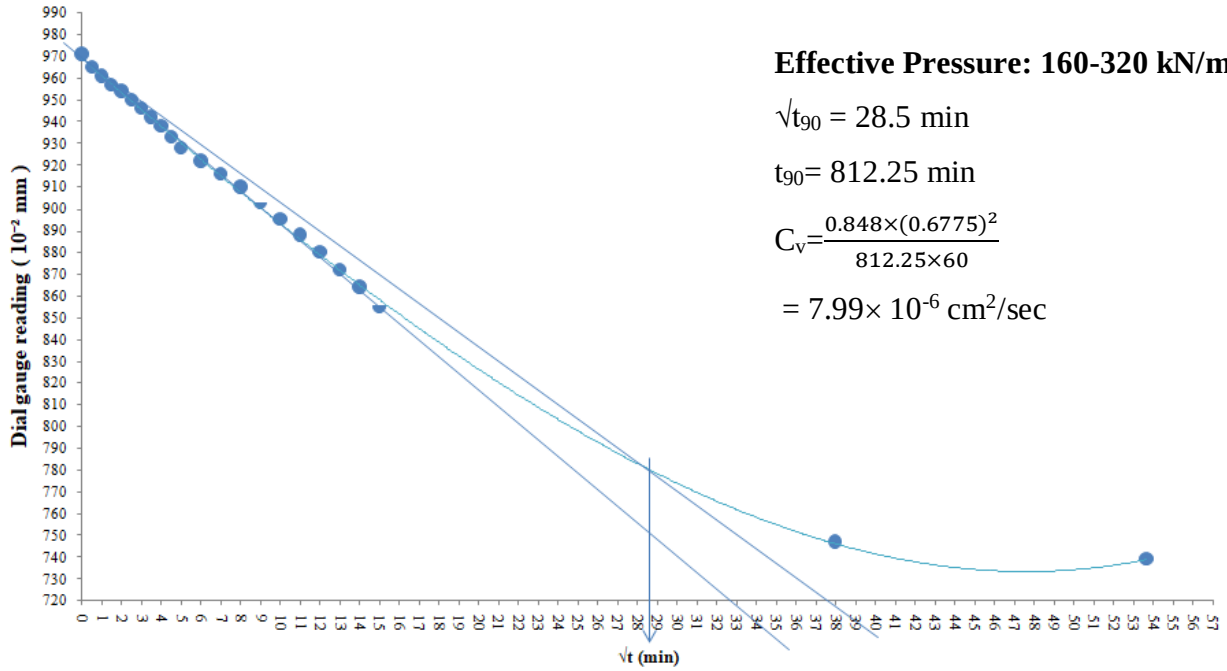

Effective Pressure: 160-320 kN/m^2

$\sqrt{t_{90}}$ = 28.5 min

t_{90}= 812.25 min

$C_v = \frac{0.848 \times (0.6775)^2}{812.25 \times 60}$

= 7.99× 10^{-6} cm^2/sec

Figure 8.10: Time vs Dial Reading graph of sample with density 1.2 gm/cc at 160-320 kN/m^2

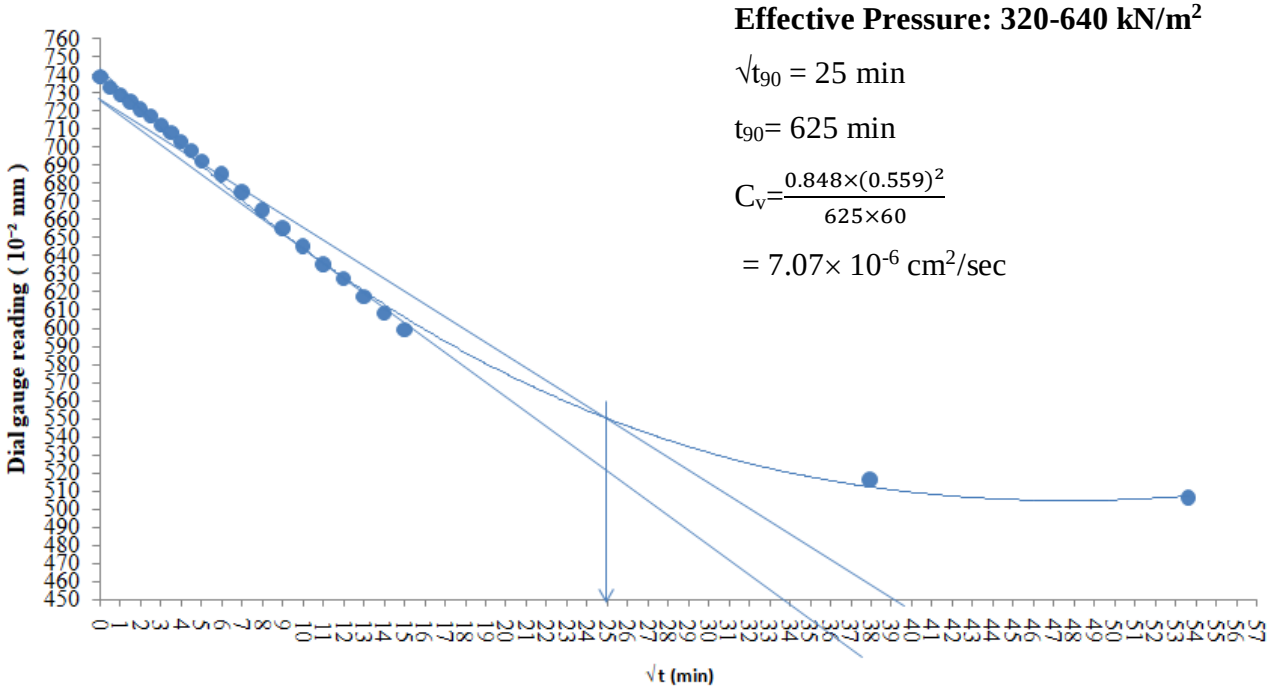

Figure 5.11: Time vs Dial Reading graph of sample with density 1.2 gm/cc at 320-640 kN/m²

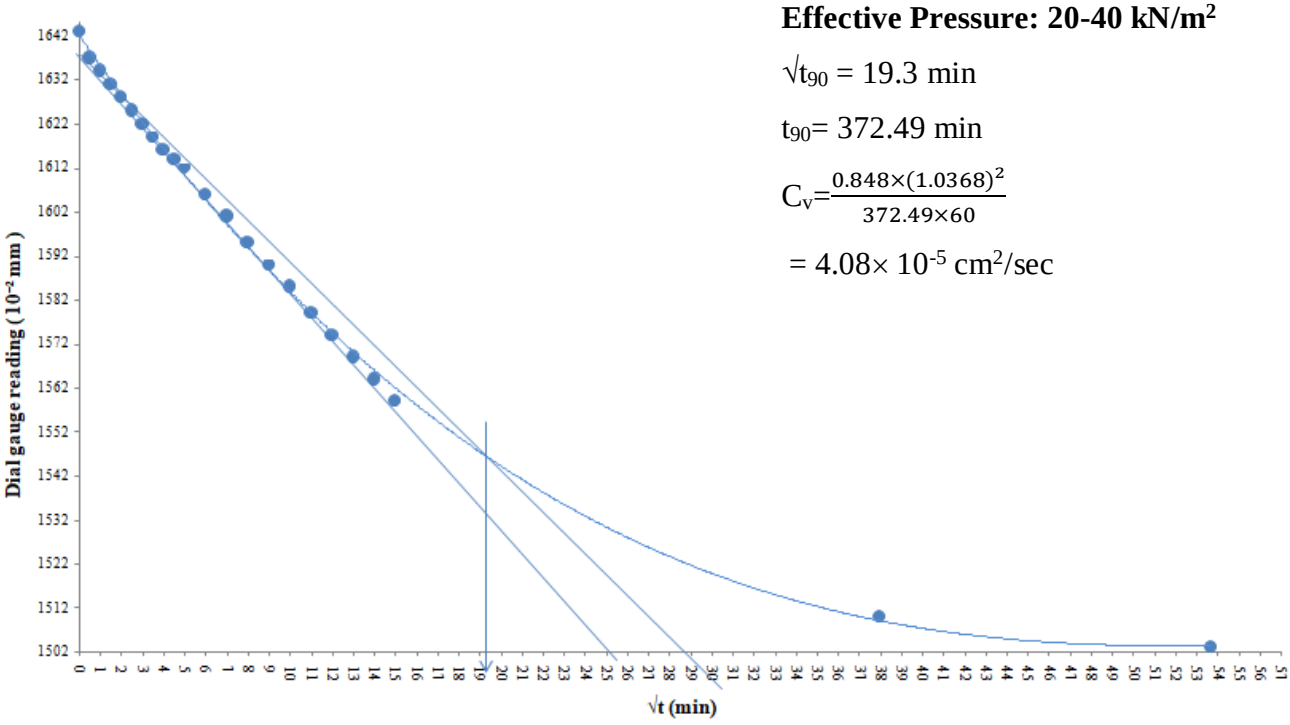

Figure 5.12: Time vs Dial Reading graph of sample with density 1.1 gm/cc at 20-40 kN/m²

Effective Pressure: 40-120 kN/m^2

$\sqrt{t_{90}}$ = 21 min

t_{90}= 441 min

$C_v = \frac{0.848 \times (0.909)^2}{441 \times 60}$

= 2.65× 10^{-5} cm^2/sec

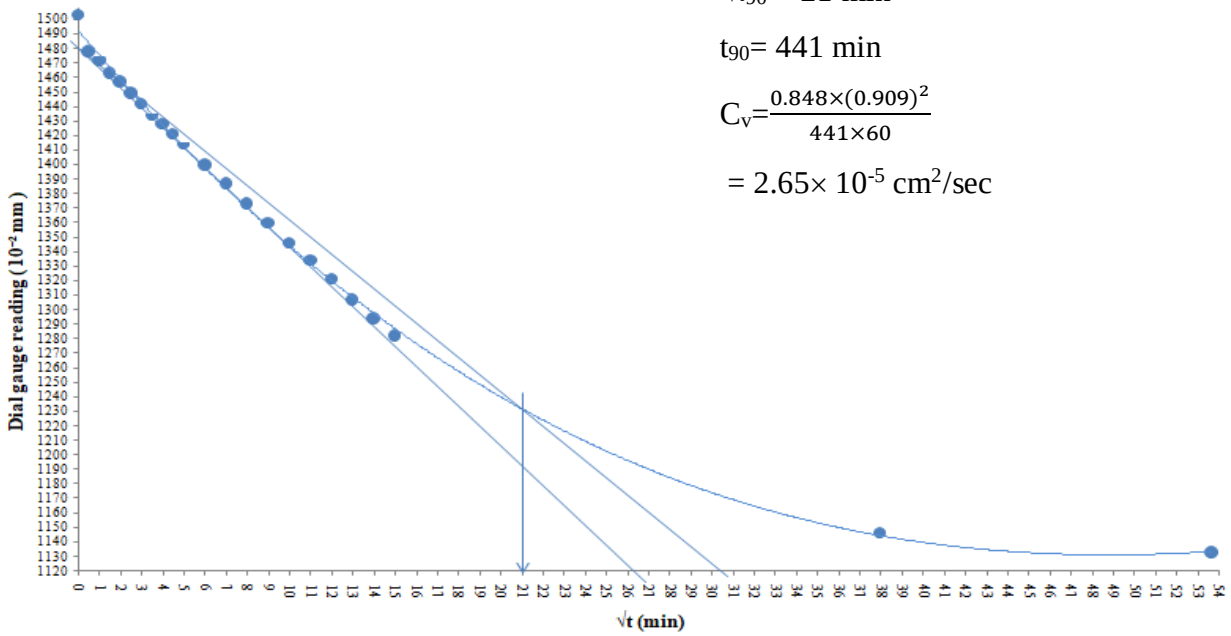

Figure 5.13: Time vs Dial Reading graph of sample with density 1.1 gm/cc at 40-120 kN/m^2

Effective Pressure: 120-160 kN/m^2

$\sqrt{t_{90}}$ = 25 min

t_{90}= 625 min

$C_v = \frac{0.848 \times (0.788)^2}{625 \times 60}$

= 1.04× 10^{-5} cm^2/sec

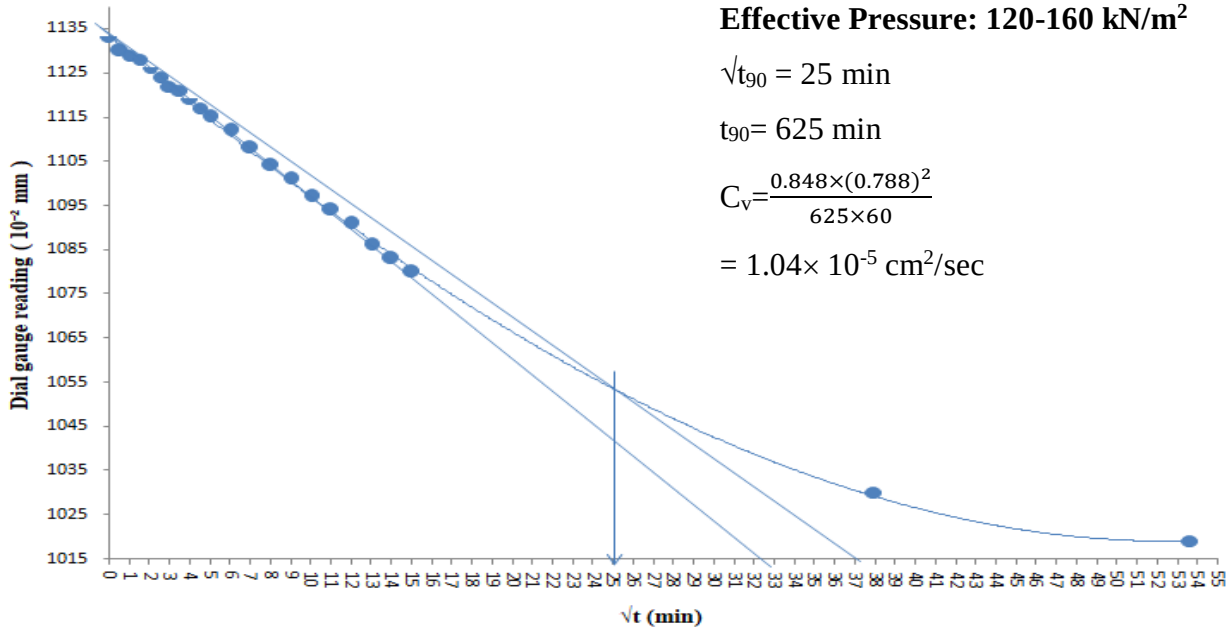

Figure 5.14: Time vs Dial Reading graph of sample with density 1.1 gm/cc at 120-160 kN/m^2

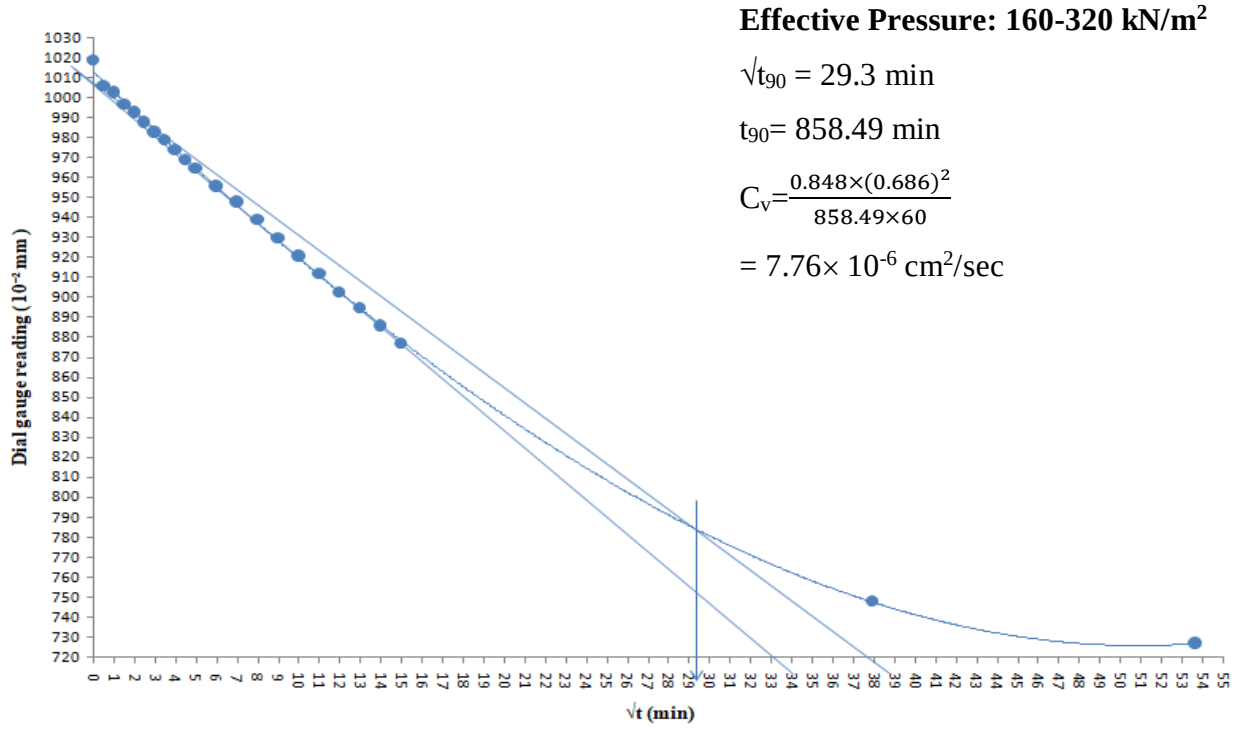

Effective Pressure: 160-320 kN/m^2

$\sqrt{t_{90}}$ = 29.3 min

t_{90}= 858.49 min

$C_v = \frac{0.848 \times (0.686)^2}{858.49 \times 60}$

= 7.76× 10^{-6} cm^2/sec

Figure 5.15: Time vs Dial Reading graph of sample with density 1.1 gm/cc at 160-320 kN/m^2

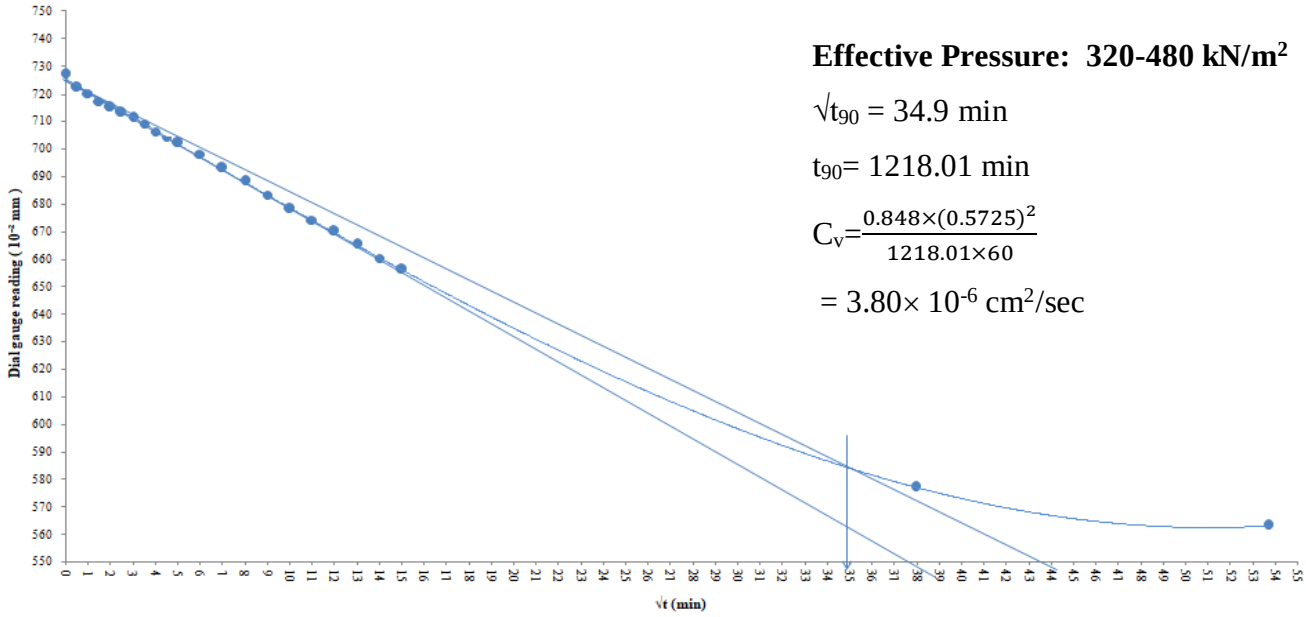

Effective Pressure: 320-480 kN/m^2

$\sqrt{t_{90}}$ = 34.9 min

t_{90}= 1218.01 min

$C_v = \frac{0.848 \times (0.5725)^2}{1218.01 \times 60}$

= 3.80× 10^{-6} cm^2/sec

Figure 5.16: Time vs Dial Reading graph of sample with density 1.1 gm/cc at 320-480 kN/m^2

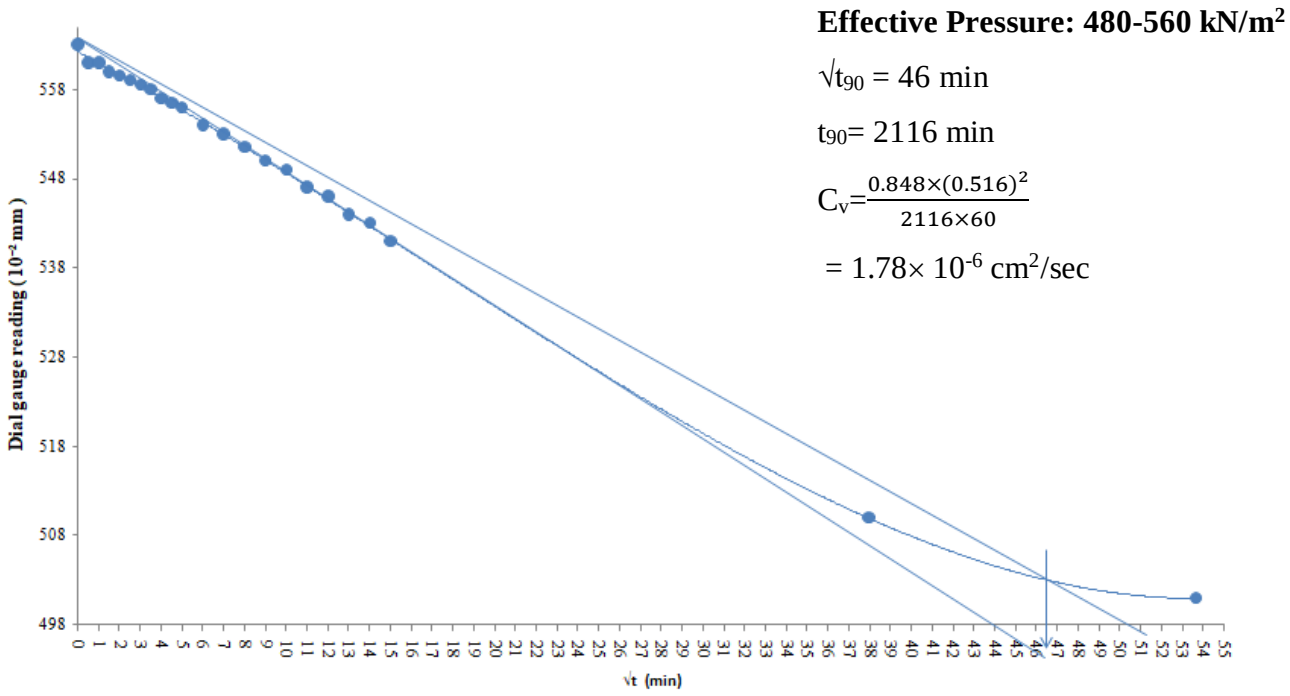

Effective Pressure: 480-560 kN/m^2

$\sqrt{t_{90}}$ = 46 min

t_{90}= 2116 min

$C_v = \frac{0.848 \times (0.516)^2}{2116 \times 60}$

= 1.78× 10^{-6} cm^2/sec

Figure 5.17: Time vs Dial Reading graph of sample with density 1.1 gm/cc at 480-560 kN/m^2

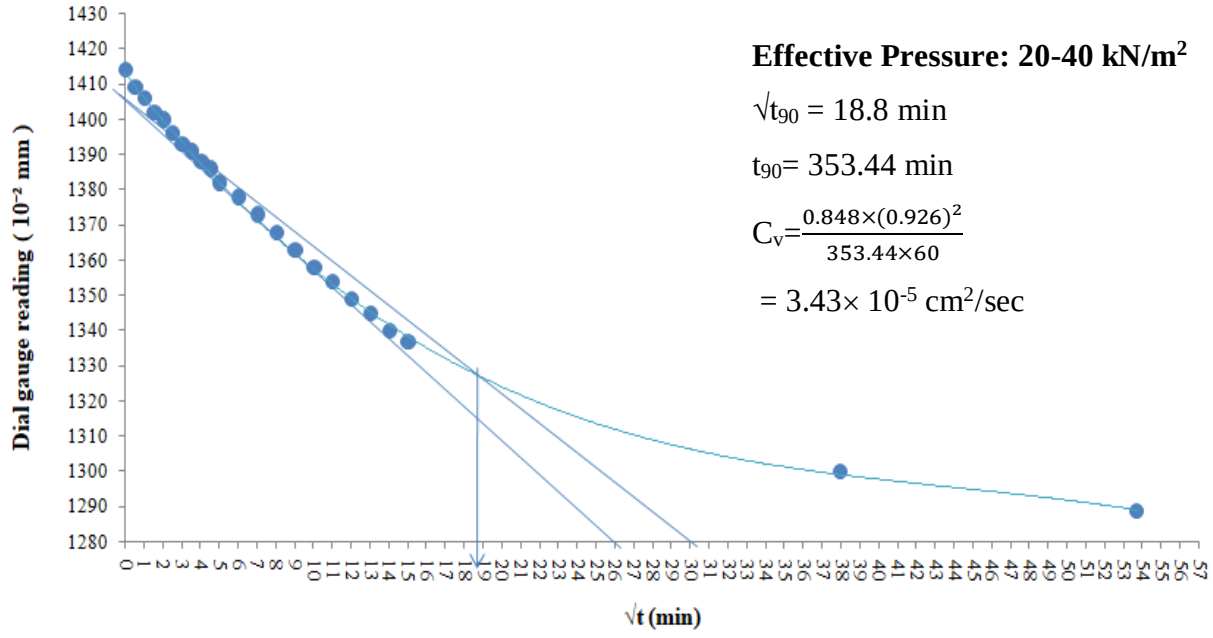

Effective Pressure: 20-40 kN/m^2

$\sqrt{t_{90}}$ = 18.8 min

t_{90}= 353.44 min

$C_v = \frac{0.848 \times (0.926)^2}{353.44 \times 60}$

= 3.43× 10^{-5} cm^2/sec

Figure 5.18: Time vs Dial Reading graph of sample with density 1.0 gm/cc at 20-40 kN/m^2

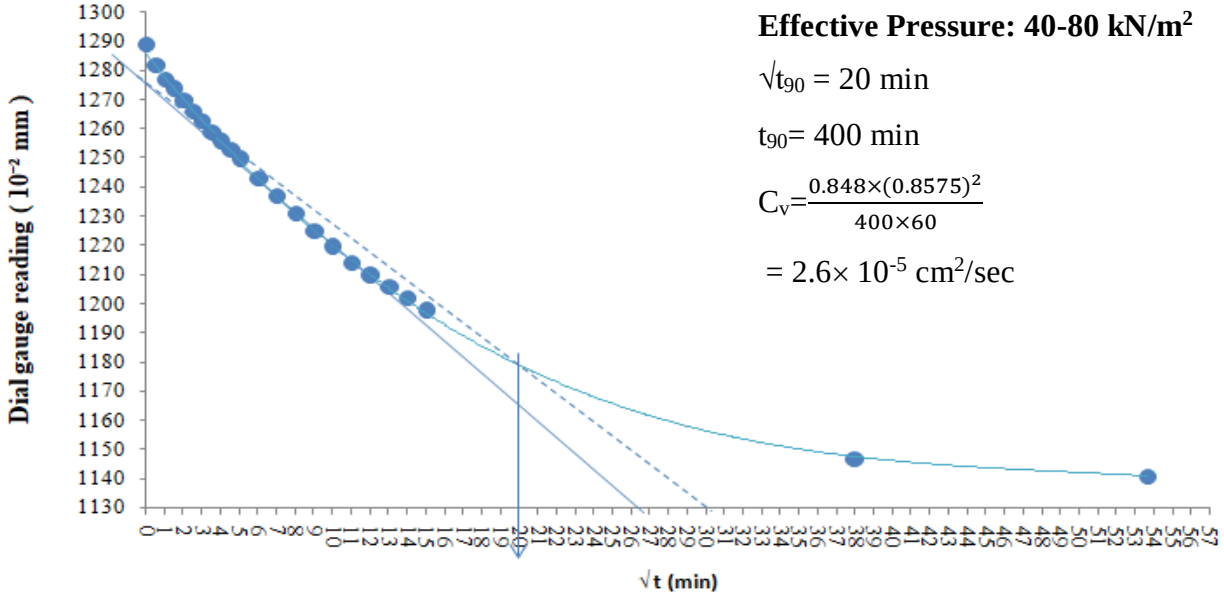

Figure 5.19: Time vs Dial Reading graph of sample with density 1.0 gm/cc at 40-80 kN/m²

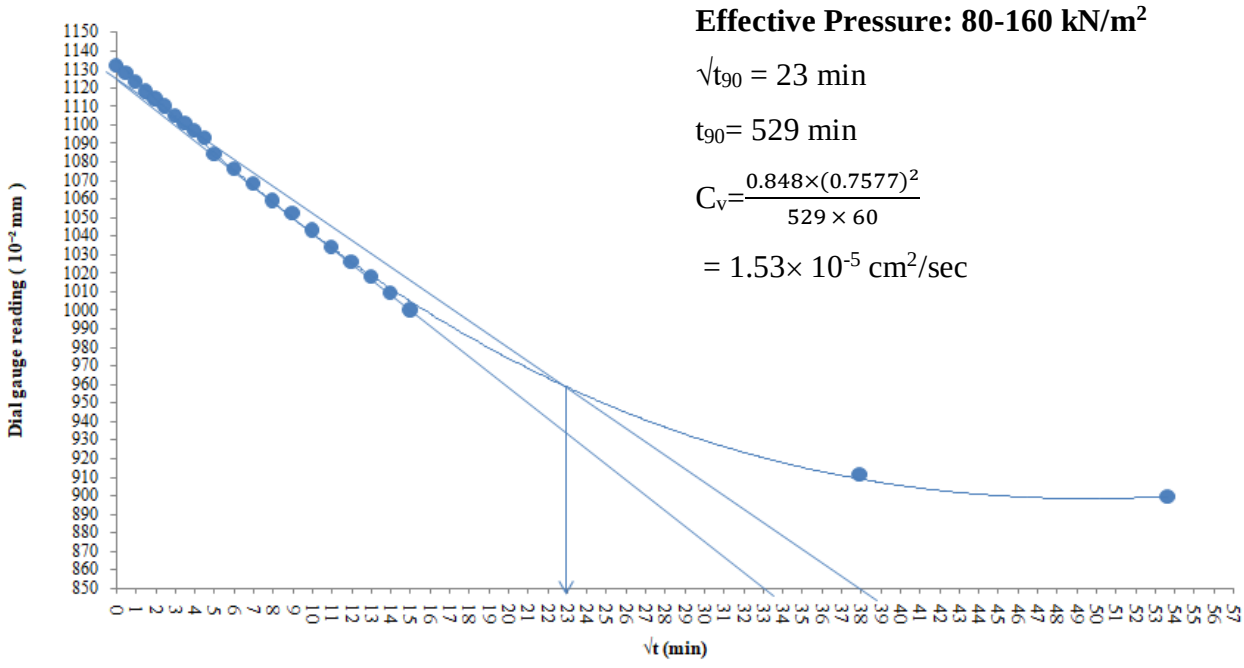

Figure 9.20: Time vs Dial Reading graph of sample with density 1.0 gm/cc at 80-160 kN/m²

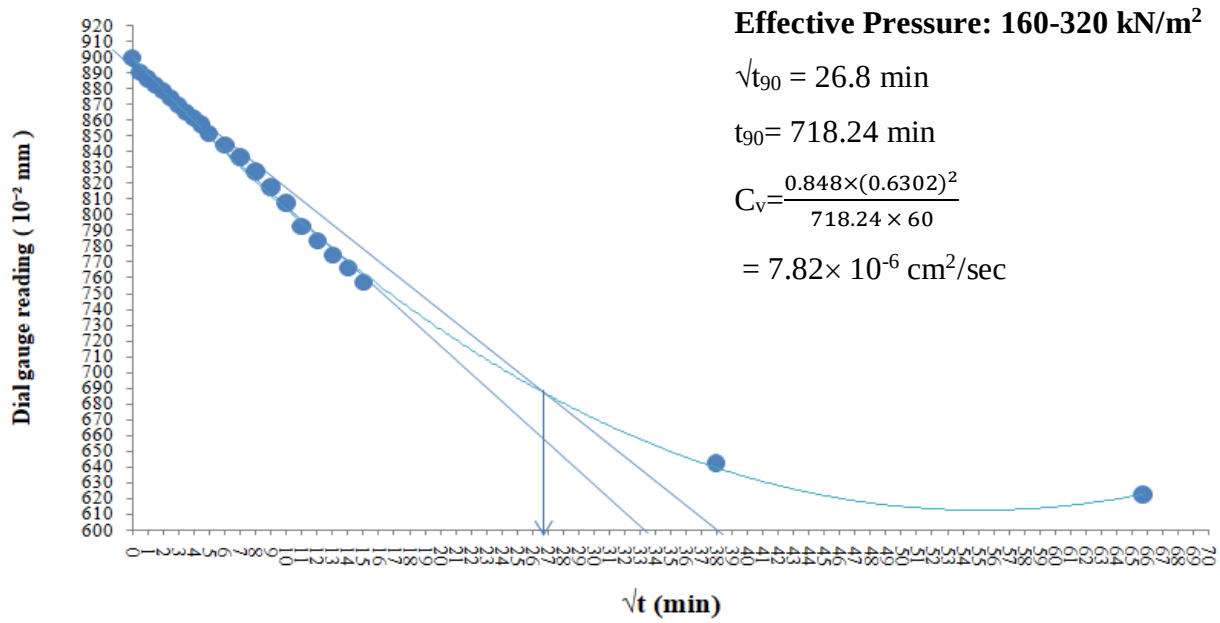

Effective Pressure: 160-320 kN/m^2

$\sqrt{t_{90}}$ = 26.8 min

t_{90}= 718.24 min

$C_v = \frac{0.848 \times (0.6302)^2}{718.24 \times 60}$

= 7.82× 10^{-6} cm^2/sec

Figure 5.21: Time vs Dial Reading graph of sample with density 1.0 gm/cc at 160-320 kN/m^2

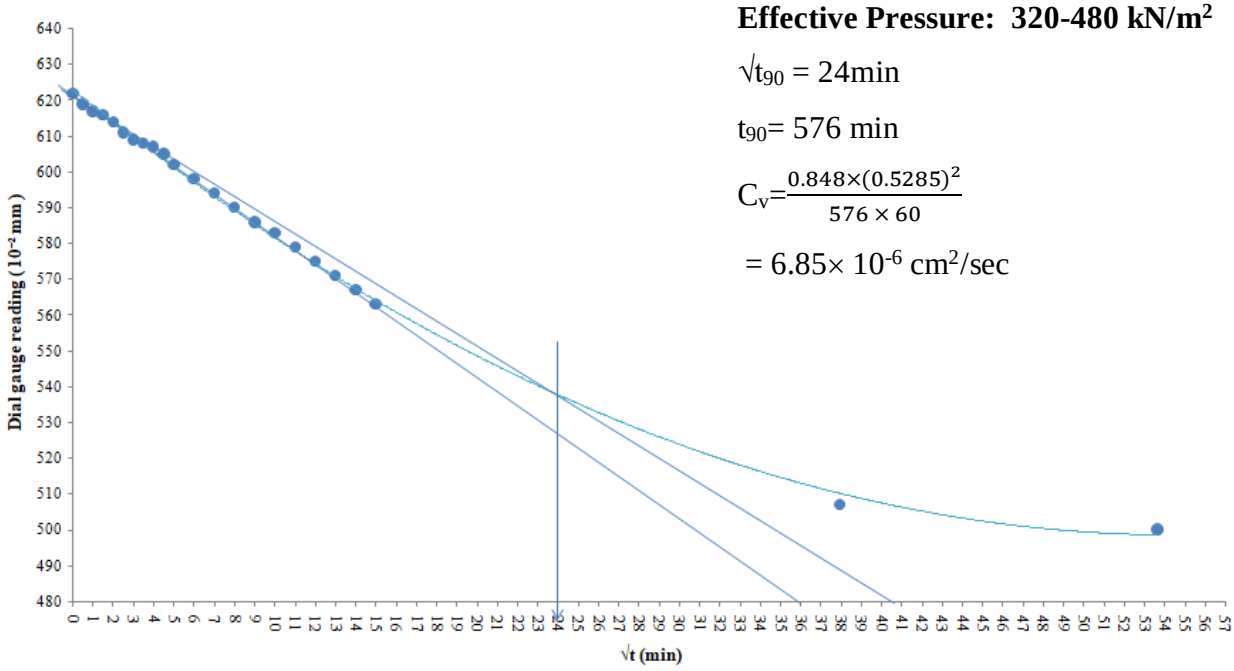

Effective Pressure: 320-480 kN/m^2

$\sqrt{t_{90}}$ = 24min

t_{90}= 576 min

$C_v = \frac{0.848 \times (0.5285)^2}{576 \times 60}$

= 6.85× 10^{-6} cm^2/sec

Figure 5.22: Time vs Dial Reading graph of sample with density 1.0 gm/cc at 320-480 kN/m^2

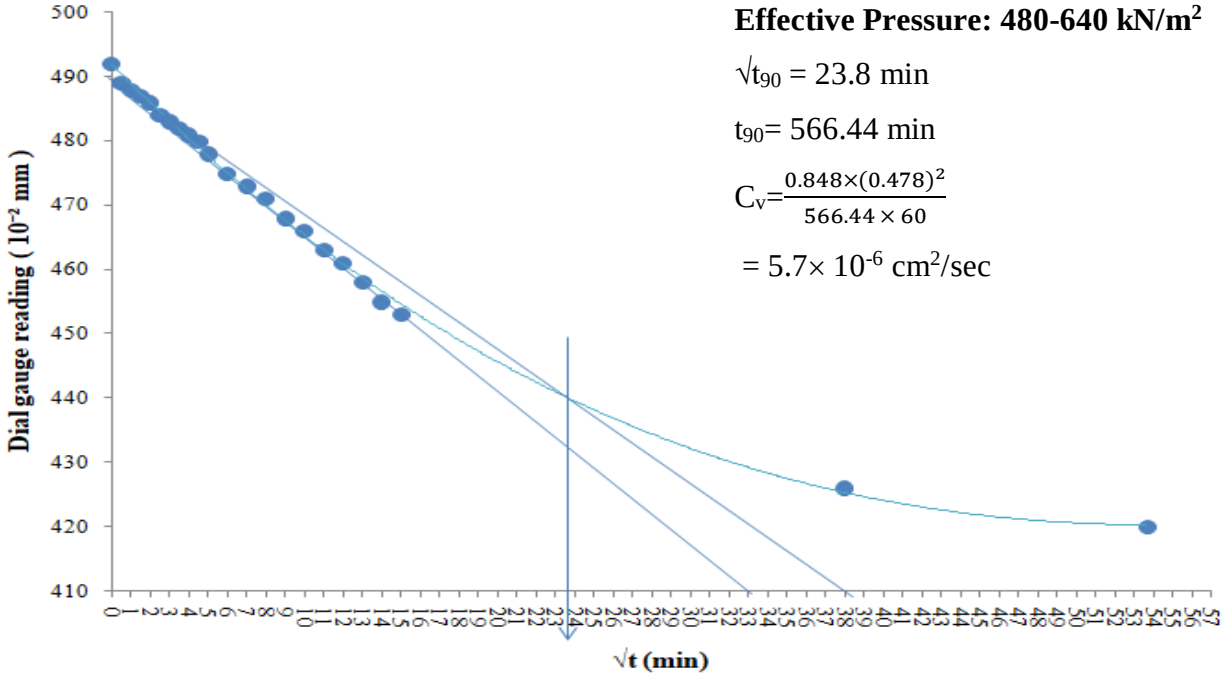

Figure 5.23: Time vs Dial Reading graph of sample with density 1.0 gm/cc at 480-640 kN/m²

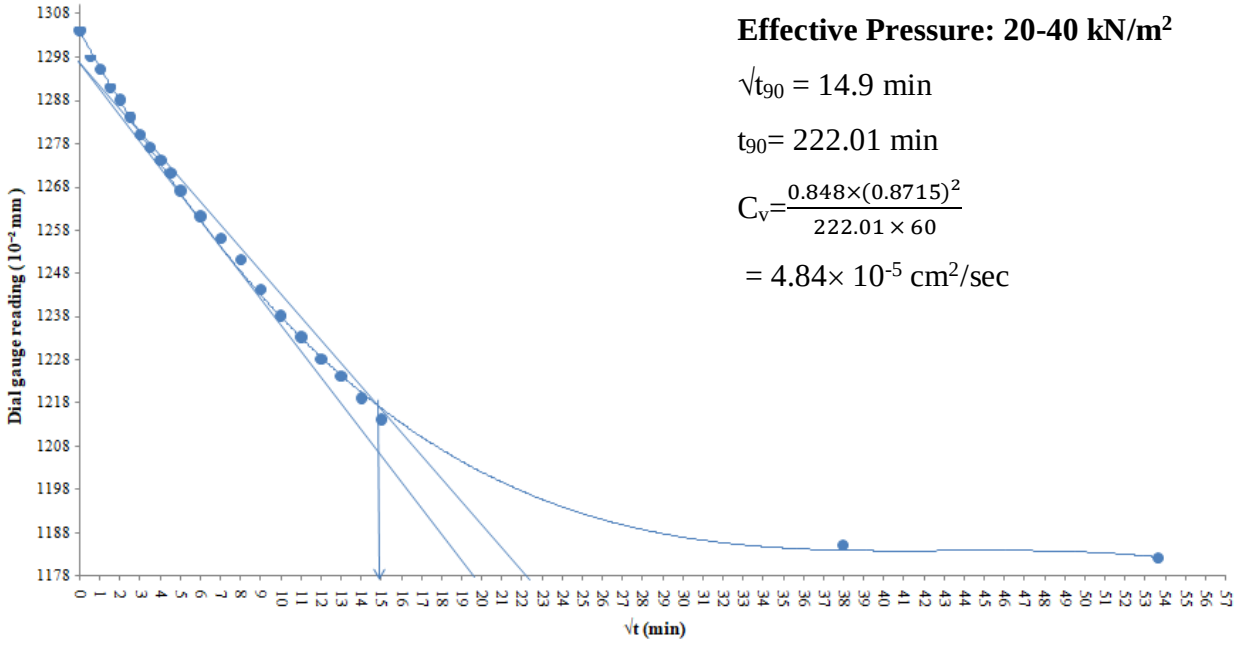

Figure 5.24: Time vs Dial Reading graph of sample with density 0.9 gm/cc at 20-40 kN/m²

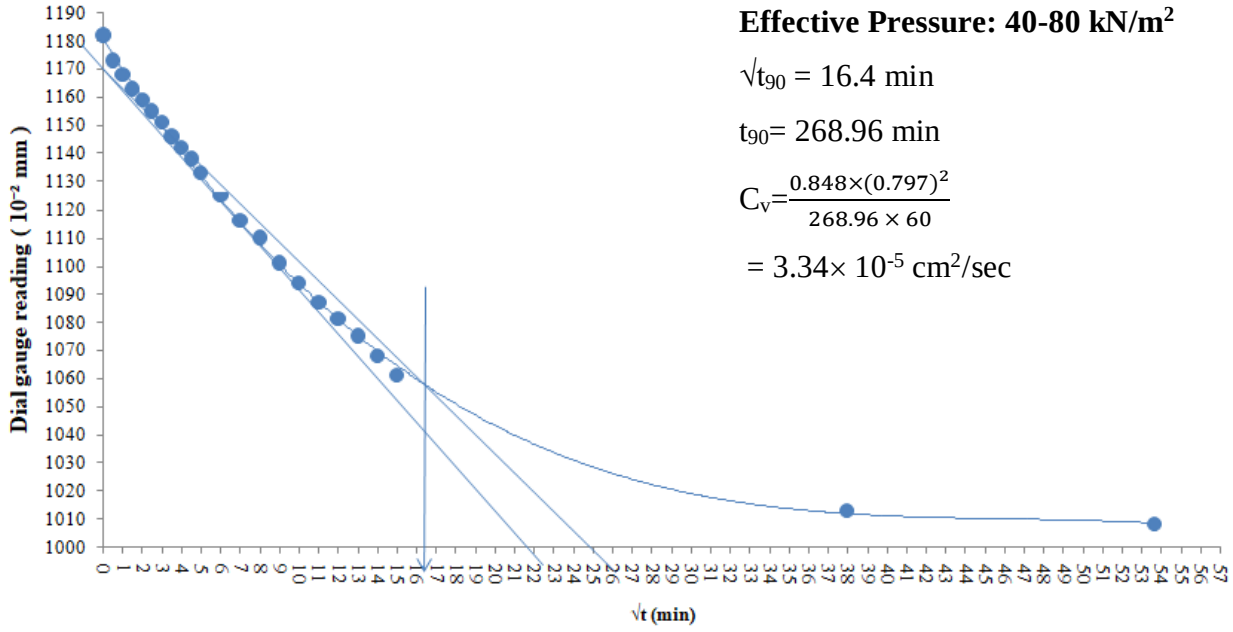

Effective Pressure: 40-80 kN/m²

$\sqrt{t_{90}}$ = 16.4 min

t_{90}= 268.96 min

$C_v = \frac{0.848 \times (0.797)^2}{268.96 \times 60}$

= 3.34× 10^{-5} cm^2/sec

Figure 5.25: Time vs Dial Reading graph of sample with density 0.9 gm/cc at 40-80 kN/m²

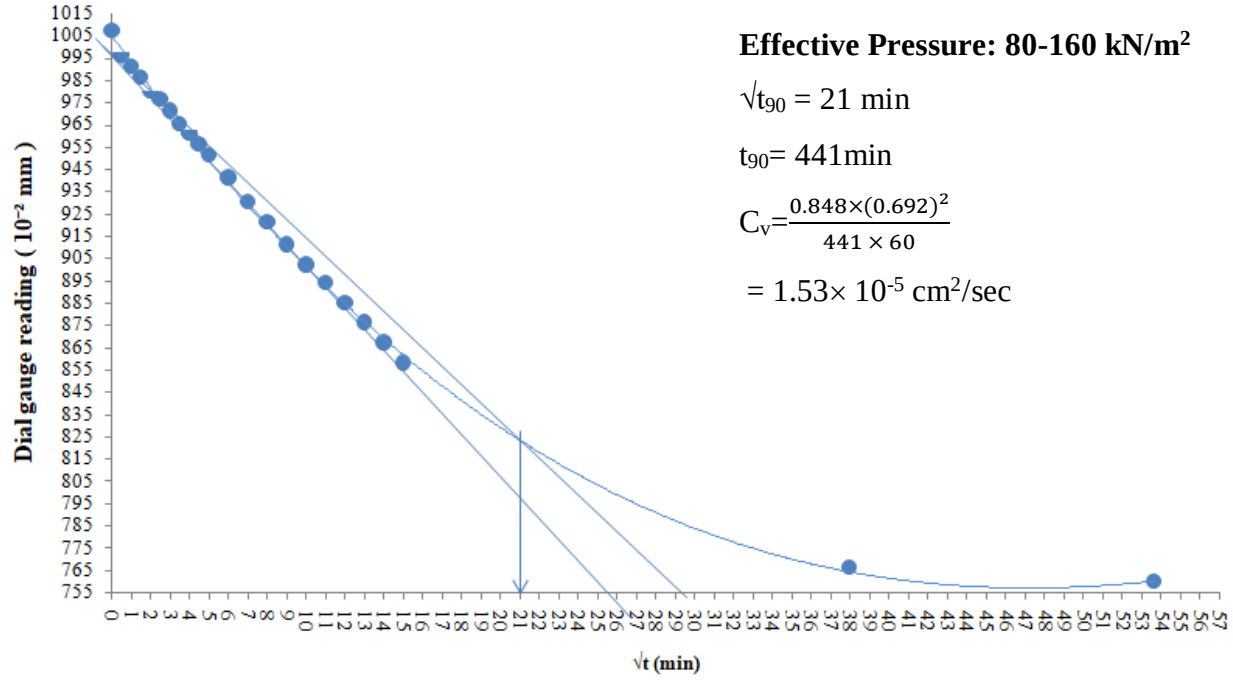

Effective Pressure: 80-160 kN/m²

$\sqrt{t_{90}}$ = 21 min

t_{90}= 441min

$C_v = \frac{0.848 \times (0.692)^2}{441 \times 60}$

= 1.53× 10^{-5} cm^2/sec

Figure 5.26: Time vs Dial Reading graph of sample with density 0.9 gm/cc at 80-160 kN/m²

Effective Pressure: 160-240kN/m^2

$\sqrt{t_{90}}$ = 20 min

t_{90}= 400 min

$C_v = \frac{0.848 \times (0.598)^2}{400 \times 60}$

= 1.27× 10^{-5} cm^2/sec

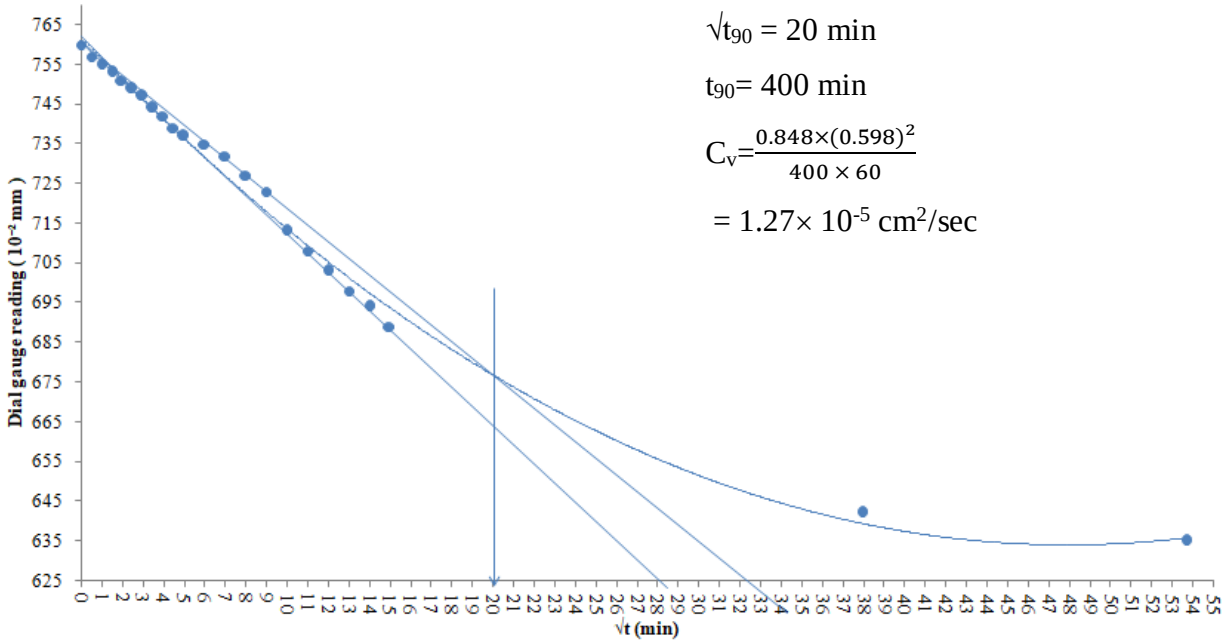

Figure 5.27: Time vs Dial Reading graph of sample with density 0.9 gm/cc at 160-240 kN/m^2

Effective Pressure: 240-320 kN/m^2

$\sqrt{t_{90}}$ = 22.4 min

t_{90}= 501.76 min

$C_v = \frac{0.848 \times (0.543)^2}{501.76 \times 60}$

= 8.31× 10^{-6} cm^2/sec

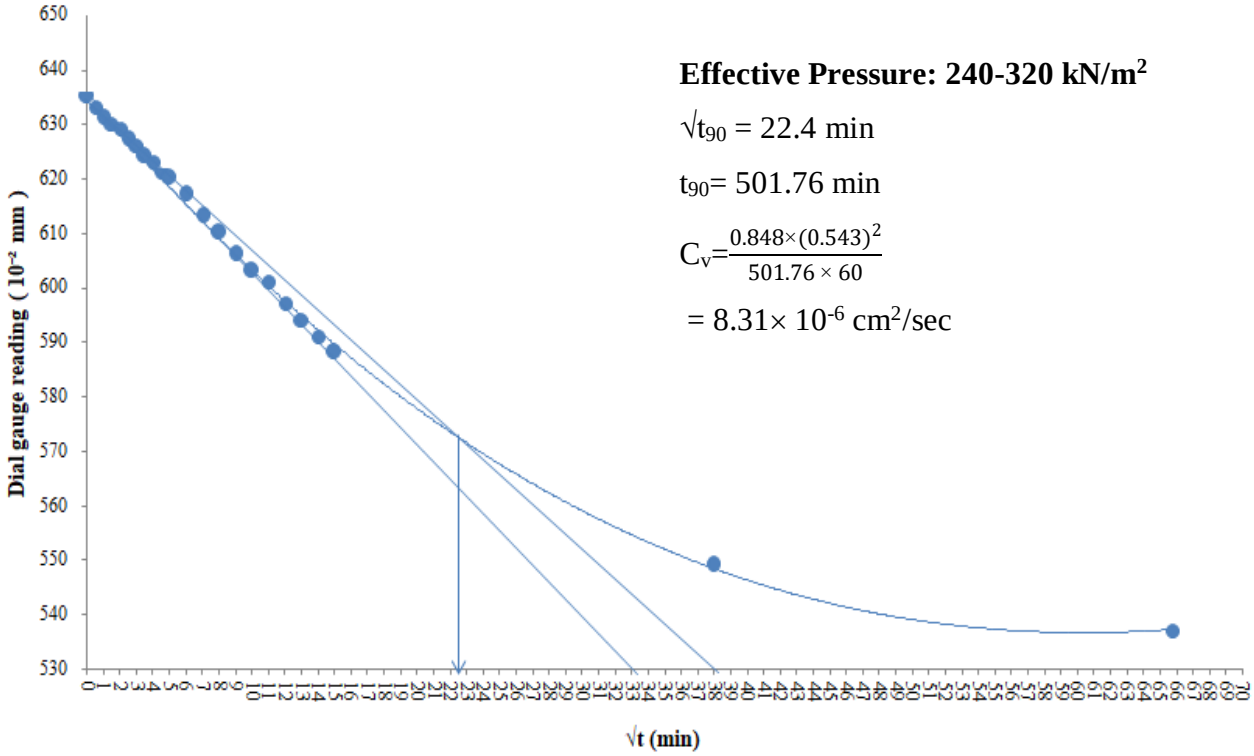

Figure 5.28: Time vs Dial Reading graph of sample with density 0.9 gm/cc at 240-320 kN/m^2

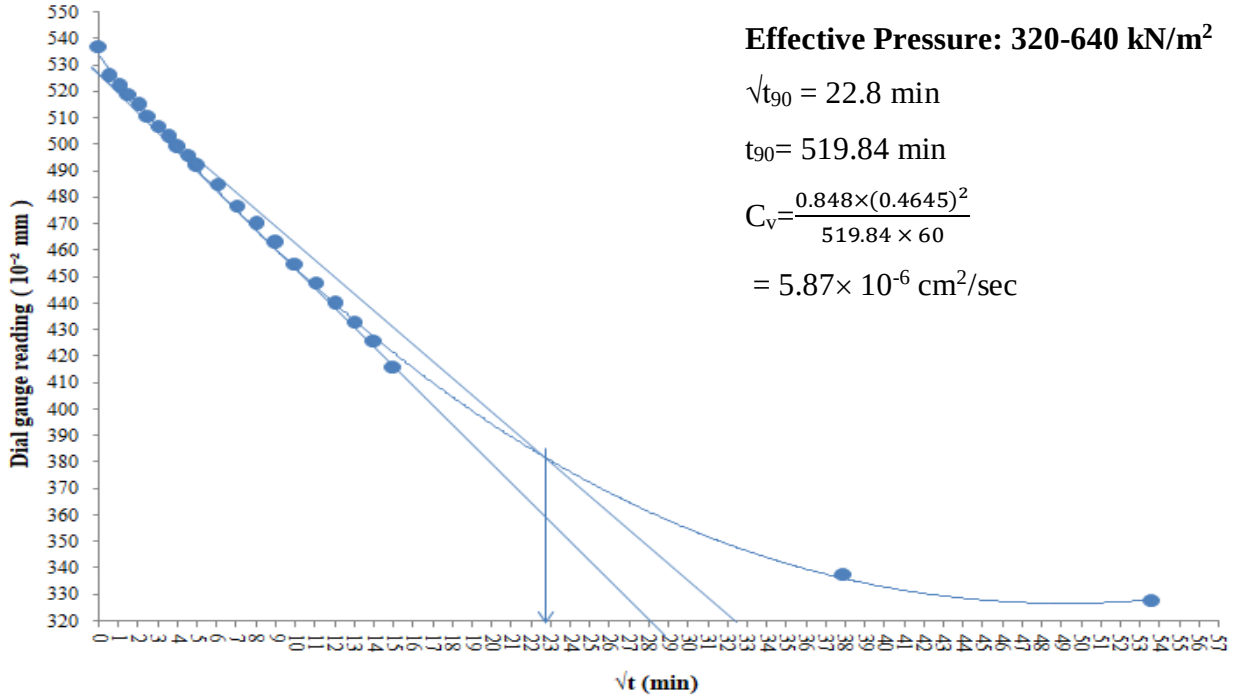

Effective Pressure: 320-640 kN/m^2

$\sqrt{t_{90}}$ = 22.8 min

t_{90}= 519.84 min

$C_v = \frac{0.848 \times (0.4645)^2}{519.84 \times 60}$

= 5.87× 10^{-6} cm^2/sec

Figure 5.29: Time vs Dial Reading graph of sample with density 0.9 gm/cc at 320-640 kN/m^2

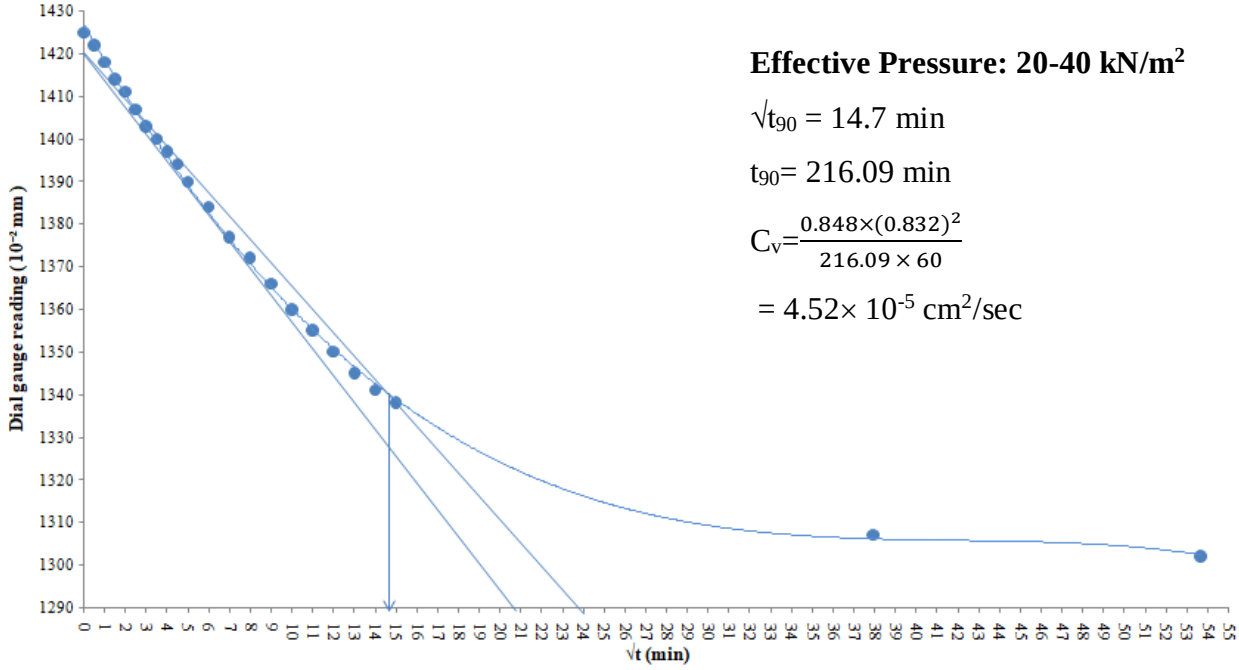

Effective Pressure: 20-40 kN/m^2

$\sqrt{t_{90}}$ = 14.7 min

t_{90}= 216.09 min

$C_v = \frac{0.848 \times (0.832)^2}{216.09 \times 60}$

= 4.52× 10^{-5} cm^2/sec

Figure 5.30: Time vs Dial Reading graph of sample with density 0.8 gm/cc at 20-40 kN/m^2

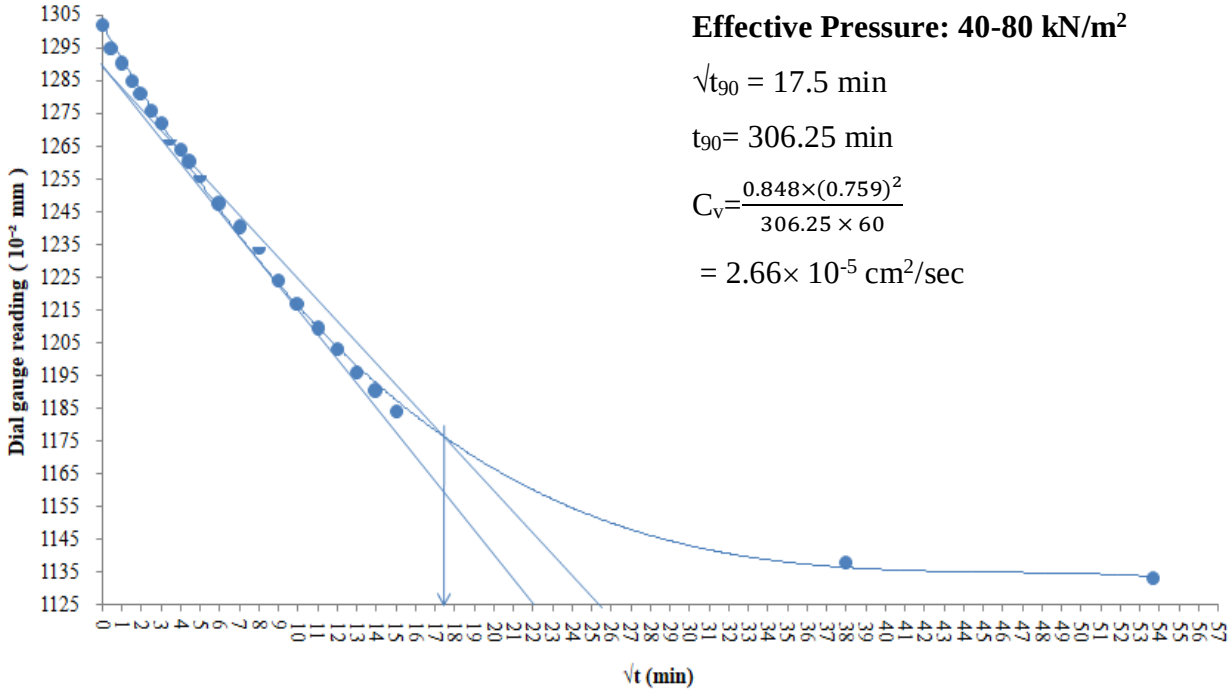

Effective Pressure: 40-80 kN/m²

$\sqrt{t_{90}}$ = 17.5 min

t_{90}= 306.25 min

$C_v = \frac{0.848 \times (0.759)^2}{306.25 \times 60}$

= 2.66× 10^{-5} cm^2/sec

Figure 5.31: Time vs Dial Reading graph of sample with density 0.8 gm/cc at 40-80kN/m²

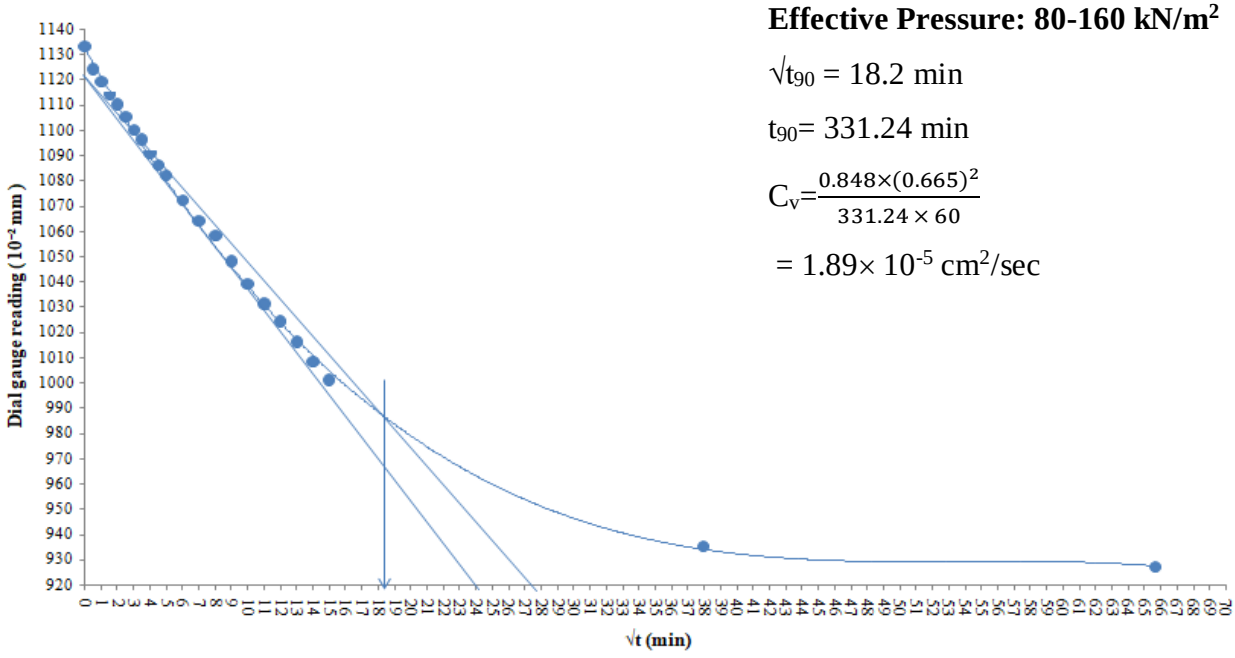

Effective Pressure: 80-160 kN/m²

$\sqrt{t_{90}}$ = 18.2 min

t_{90}= 331.24 min

$C_v = \frac{0.848 \times (0.665)^2}{331.24 \times 60}$

= 1.89× 10^{-5} cm^2/sec

Figure 5.32: Time vs Dial Reading graph of sample with density 0.8 gm/cc at 80-160kN/m²

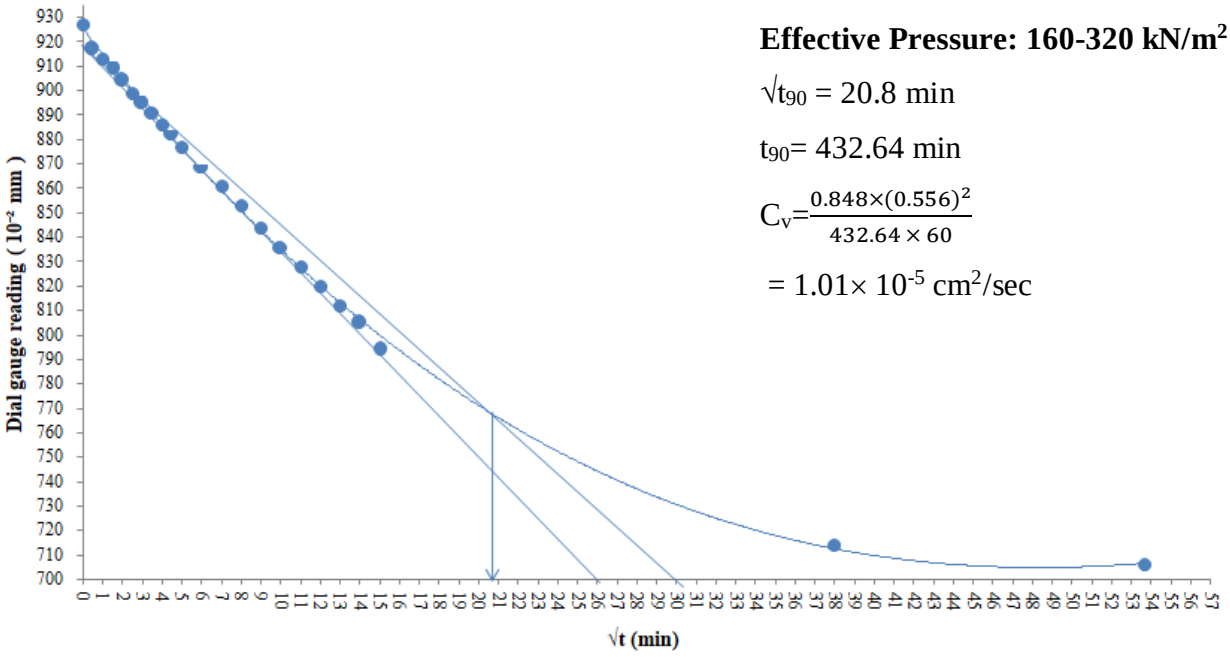

Effective Pressure: 160-320 kN/m^2

$\sqrt{t_{90}}$ = 20.8 min

t_{90}= 432.64 min

$C_v = \frac{0.848 \times (0.556)^2}{432.64 \times 60}$

= 1.01× 10^{-5} cm^2/sec

Figure 5.33: Time vs Dial Reading graph of sample with density 0.8 gm/cc at 160-320kN/m^2

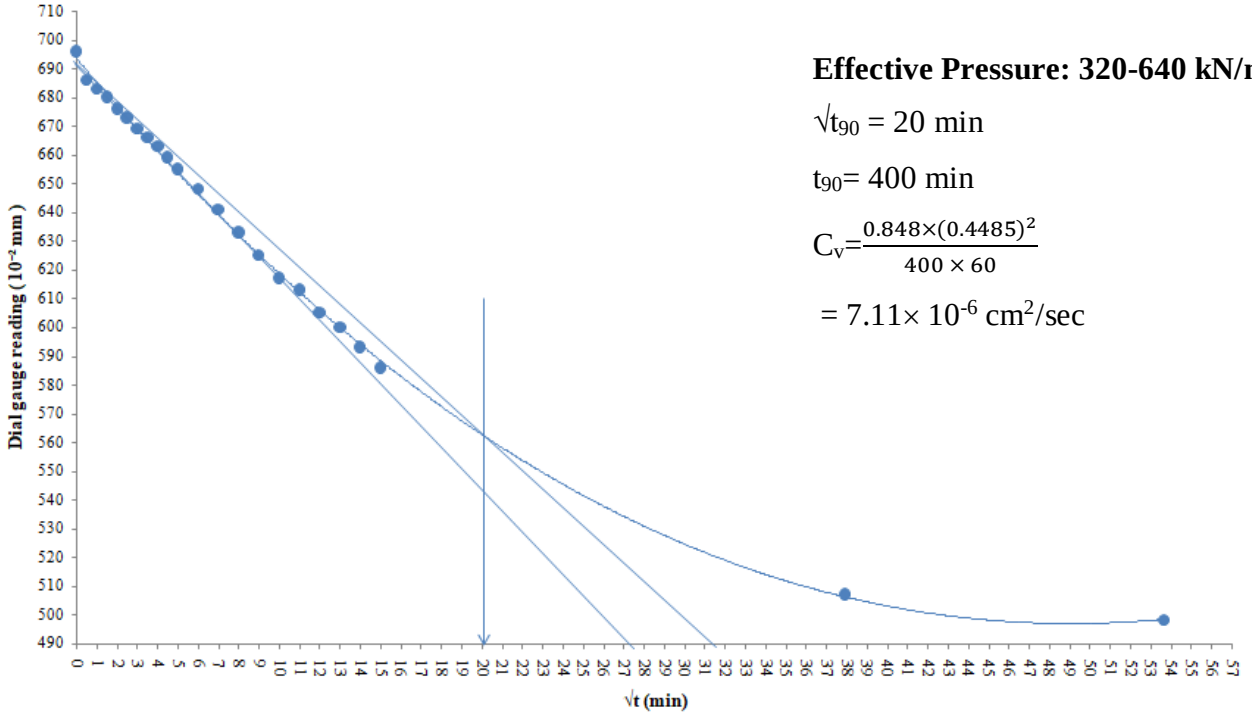

Effective Pressure: 320-640 kN/m^2

$\sqrt{t_{90}}$ = 20 min

t_{90}= 400 min

$C_v = \frac{0.848 \times (0.4485)^2}{400 \times 60}$

= 7.11× 10^{-6} cm^2/sec

Figure 5.34: Time vs Dial Reading graph of sample with density 0.8 gm/cc at 320-640kN/m^2

Table 5.4: Consolidation Characteristics of granulated bentonite permeated with distilled water at 1.2 gm/cc

Applied pressure (kN/m^2)	Void Ratio (e)	Coefficient of compressibility, (a_v) (m^2/kN)	Coefficient of volume change, (m_v) (m^2/kN)	Coefficient of consolidation, (C_v) (cm^2/sec)	Coefficient of permeability, (k) (cm/sec)
10	5.47				
20	5.19	0.0283	0.0044		
40	4.59	0.0301	0.0049	1.58E-05	7.50E-09
80	3.93	0.0166	0.0030	1.30E-05	3.78E-09
160	3.26	0.0084	0.0017	9.89E-06	1.65E-09
320	2.59	0.0042	0.0010	7.99E-06	7.71E-10
640	1.91	0.0021	0.0006	7.07E-06	4.07E-10

Table 5.3: Consolidation Characteristics of granulated bentonite permeated with distilled water at 1.1gm/cc

Applied pressure (kN/m^2)	Void Ratio (e)	Coefficient of compressibility, (a_v) (m^2/kN)	Coefficient of volume change, (m_v) (m^2/kN)	Coefficient of consolidation, (C_v) (cm^2/sec)	Coefficient of permeability, (k) (cm/sec)
10	5.38				
20	5.14	0.0241	0.0038		
40	4.74	0.0201	0.0033	4.08E-05	1.31E-08
120	3.68	0.0133	0.0023	2.65E-05	6.00E-09
160	3.35	0.0082	0.0017	1.40E-05	2.40E-09
320	2.52	0.0052	0.0012	7.76E-06	9.14E-10
480	2.05	0.0029	0.0008	3.80E-06	3.12E-10
560	1.87	0.0022	0.0007	1.75E-06	1.25E-10

Table 5.4: Consolidation Characteristics of granulated bentonite permeated with distilled water at 1.0gm/cc

Applied pressure (kN/m^2)	Void Ratio (e)	Coefficient of compressibility, (a_v) (m^2/kN)	Coefficient of volume change, (m_v) (m^2/kN)	Coefficient of consolidation, (C_v) (cm^2/sec)	Coefficient of permeability, (k) (cm/sec)
10	5.18				
20	5.02	0.0160	0.0026		
40	4.63	0.0197	0.0033	3.43E-05	1.10E-08
80	4.16	0.0116	0.0021	2.60E-05	5.27E-09
160	3.40	0.0095	0.0018	1.53E-05	2.77E-09
320	2.53	0.0054	0.0012	7.82E-06	9.49E-10
480	2.14	0.0024	0.0007	6.85E-06	4.57E-10
640	1.89	0.0016	0.0005	5.70E-06	2.80E-10

Table 5.5: Consolidation Characteristics of granulated bentonite permeated with distilled water at 0.9gm/cc

Applied pressure (kN/m^2)	Void Ratio (e)	Coefficient of compressibility, (a_v) (m^2/kN)	Coefficient of volume change, (m_v) (m^2/kN)	Coefficient of consolidation, (C_v) (cm^2/sec)	Coefficient of permeability, (k) (cm/sec)
10	5.52				
20	5.29	0.0230	0.0035		
40	4.86	0.0213	0.0034	4.84E-05	1.60E-08
80	4.25	0.0152	0.0026	3.34E-05	8.52E-09
160	3.39	0.0108	0.0020	1.53E-05	3.08E-09
240	2.95	0.0054	0.0012	1.27E-05	1.54E-09
320	2.61	0.0043	0.0011	8.31E-06	8.79E-10
640	1.89	0.0023	0.0006	5.87E-06	3.62E-10

Table 5.6: Consolidation Characteristics of granulated bentonite permeated with distilled water at 0.8gm/cc

Applied pressure (kN/m^2)	Void Ratio (e)	Coefficient of compressibility, (a_v) (m^2/kN)	Coefficient of volume change, (m_v) (m^2/kN)	Coefficient of consolidation, (C_v) (cm^2/sec)	Coefficient of permeability, (k) (cm/sec)
10	6.02				
20	5.74	0.0277	0.0040		
40	5.26	0.0240	0.0036	4.52E-05	1.58E-08
80	4.60	0.0165	0.0026	2.66E-05	6.87E-09
160	3.79	0.0101	0.0018	1.89E-05	3.33E-09
320	2.93	0.0054	0.0011	1.01E-05	1.11E-09
640	2.12	0.0025	0.0006	7.11E-06	4.50E-10

From the table 5.2- 5.6 and Figure 5.7 – 5.34, the coefficient of consolidation (C_v) of granulated bentonite decreases with increasing soil density and effective pressure, indicating slower pore water dissipation in denser soils with lower void ratios. For example, at 40 kN/m^2, C_v is 1.58×10^{-5} cm^2/sec for a density of 1.2 gm/cc and 4.52×10^{-5} cm^2/sec for 0.8 gm/cc. Similarly, C_v decreases with permeability (k), as seen at 40 kN/m^2, where k is 7.50×10^{-9} cm/sec for 1.2 gm/cc, reducing to 7.71×10^{-10}cm/sec at 320 kN/m^2. Lower-density soils with higher void ratios exhibit higher $C_v$and k, while denser soils show reduced values due to compaction. This highlights the strong influence of permeability and density on consolidation rates.

CHAPTER 6

Analysis of Permeability Behaviour of Granulated Bentonite

6.1 General

Permeability is the property of a material that measures its ability to allow fluids to pass through it, quantifying the ease with which water or other liquids flow through porous materials like soil or rock. It is typically expressed as a coefficient in units of velocity (e.g., cm/s). In landfill liners, permeability plays a critical role in controlling the migration of leachate—a liquid generated by waste decomposition and water infiltration—into the surrounding soil and groundwater. Low permeability is essential to minimize leachate seepage, ensuring environmental safety and compliance with regulations. Understanding the permeability of liner materials is crucial for designing effective landfill systems, as it helps protect groundwater by preventing contaminant migration, maintains the structural integrity of the liner by reducing leachate pressure, and ensures compliance with regulatory standards. Evaluating permeability is, therefore, fundamental to selecting appropriate liner materials and achieving long-term environmental sustainability in landfill operations.

6.2 Determination of Coefficient of Permeability (k)

The coefficient of permeability of a soil describes how easily a liquid will move through a soil. It is also commonly referred to as the hydraulic conductivity of a soil. Once we have the values for m_v and C_v, the following equation to determine the value of k:

$k = C_v \times m_v \times \gamma_w$ ...(6.1)

Where, k= Hydraulic conductivity

C_v = coefficient of consolidation

m_v = coefficient of volume compressibility

γ_w = unit weight of water.

6.3 Analysis of Permeability behaviour of granulated bentonite of different densities

The permeability behavior of granulated bentonite at varying densities was analyzed using a one-dimensional consolidometer apparatus. Dry granulated bentonite samples, prepared by weight, were compacted to densities of 1.2, 1.1, 1.0, 0.9, and 0.8 g/cm³ maintaining a sample height of

10 mm within the cutter. Filter papers were placed at the top and bottom of the samples, and porous stones, pre-boiled for 15 minutes, were positioned above and below the filter papers.

An initial seating load of 5 kN/m² was applied via the loading hanger at the beginning of the test. The saturation of the dry soil samples was carried out using distilled water. Due to the highly expansive nature of the soil, the samples were allowed to swell completely before further testing. Once full swelling is achieved, the application of overburden stress begins, starting at 10 kN/m² and increasing incrementally in a doubling sequence (e.g., 10, 20, 40, 80, 160, 320, and 640 kN/m²). From 40 kN/m² onward, dial gauge readings are recorded over time in accordance with IS 2720 Part XV with observations taken for up to 48 hours. Distilled water (pore fluid) is continuously supplied to ensure the sample remains saturated throughout the process. The permeability characteristics are determined from 40 kN/m² to 640 kN/m², with the same procedure followed for each subsequent load increment.

6.3.1 Variation of the permeability with void ratio

The permeability variation of granulated bentonite samples saturated with distilled water at densities of 1.2, 1.1, 1.0, 0.9, and 0.8 g/cm³ is summarized in Tables 6.1 to 6.5, with the corresponding graphs illustrated in Figures 6.1 to 6.5. Additionally, Figure 6.6 presents the combined graphs of void ratio versus permeability for all densities.

Table 6.5: Applied Pressure, Void Ratio and Coefficient of permeability for density 1.2 gm/cc

Density - 1.2 gm/cc		
Applied Pressure (kN/m2)	**Void Ratio**	**Coefficient Of Permeability (cm/s)**
40	4.59	7.50E-09
80	3.93	3.78E-09
120	3.59	2.72E-09
160	3.26	1.65E-09
240	2.92	1.21E-09
320	2.59	7.71E-10
440	2.33	6.35E-10
480	2.25	5.89E-10
560	2.08	4.98E-10
640	1.91	4.07E-10

Table 6.6: Applied Pressure, Void Ratio and Coefficient of permeability for density 1.1 gm/cc

Density -1.1gm/cc		
Applied Pressure (kN/m2)	**Void Ratio**	**Coefficient Of Permeability (cm/s)**
40	4.74	1.31E-08
80	4.21	9.53E-09
120	3.68	6.00E-09
160	3.35	2.40E-09
240	2.93	1.66E-09
320	2.52	9.14E-10
440	2.16	4.62E-10
480	2.05	3.12E-10
560	1.87	1.25E-10
640	1.77	1.23E-10

Table 6.7: Applied Pressure, Void Ratio and Coefficient of permeability for density 1.0 gm/cc

Density -1.0gm/cc		
Applied Pressure (kN/m2)	**Void Ratio**	**Coefficient Of Permeability (cm/s)**
40	4.63	1.10E-08
80	4.16	5.27E-09
120	3.78	4.02E-09
160	3.40	2.77E-09
240	2.96	1.86E-09
320	2.53	9.49E-10
440	2.24	5.80E-10
480	2.14	4.57E-10
560	2.02	3.68E-10
640	1.89	2.80E-10

Table 6.8: Applied Pressure, Void Ratio and Coefficient of permeability for density 0.9 gm/cc

Density -0.9 gm/cc		
Applied Pressure (kN/m2)	**Void Ratio**	**Coefficient Of Permeability (cm/s)**
40	4.86	1.60E-08
80	4.25	8.52E-09
120	3.82	5.80E-09
160	3.39	3.08E-09
240	2.95	1.54E-09
320	2.61	8.79E-10
440	2.34	6.86E-10
480	2.25	6.21E-10
560	2.07	4.92E-10
640	1.89	3.62E-10

Table 6.9: Applied Pressure, Void Ratio and Coefficient of permeability for density 0.8 gm/cc

Density -0.8 gm/cc		
Applied Pressure (kN/m2)	**Void Ratio**	**Coefficient Of Permeability (cm/s)**
40	5.26	1.58E-08
80	4.60	6.87E-09
120	4.20	5.10E-09
160	3.79	3.33E-09
240	3.36	2.22E-09
320	2.93	1.11E-09
440	2.63	8.65E-10
480	2.52	7.82E-10
560	2.32	6.16E-10
640	2.12	4.50E-10

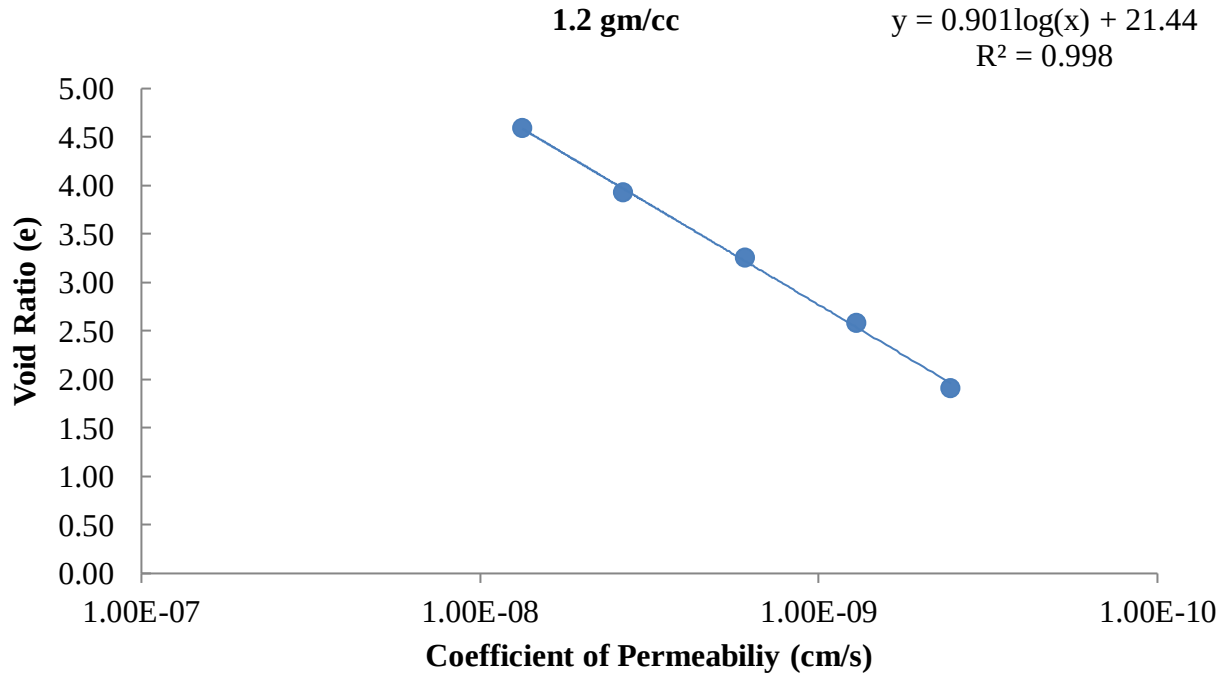

Figure 6.1: e vs log k of density 1.2 gm/cc

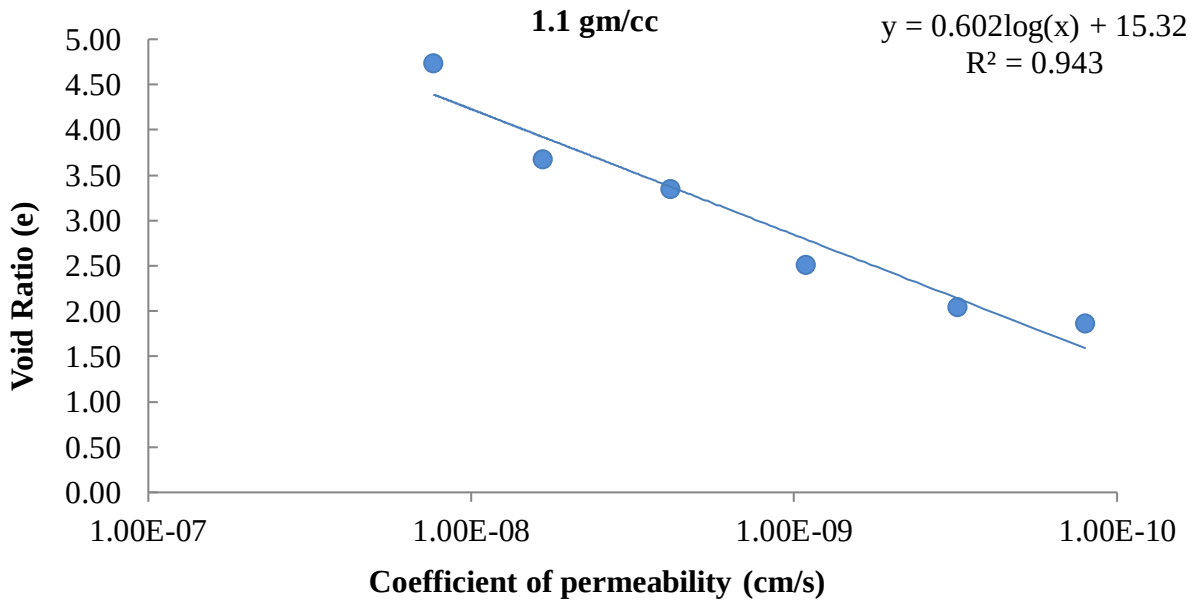

Figure 6.2: e vs log k of density 1.1 gm/cc

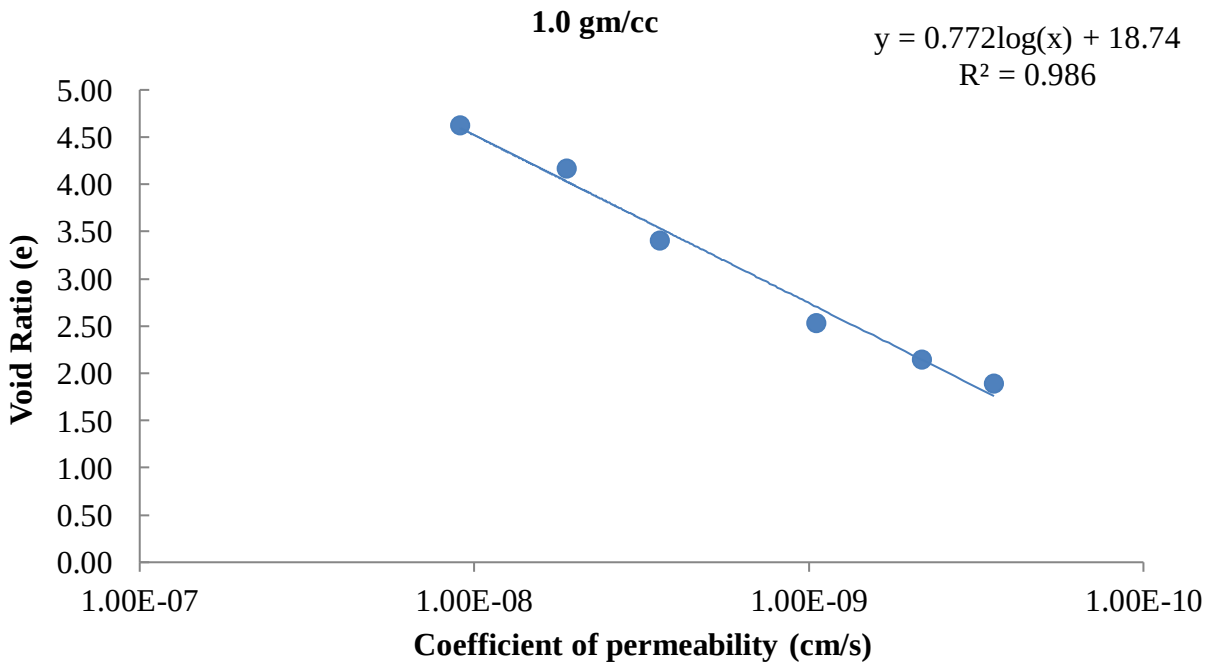

Figure 6.3: e vs log k of density 1.0 gm/cc

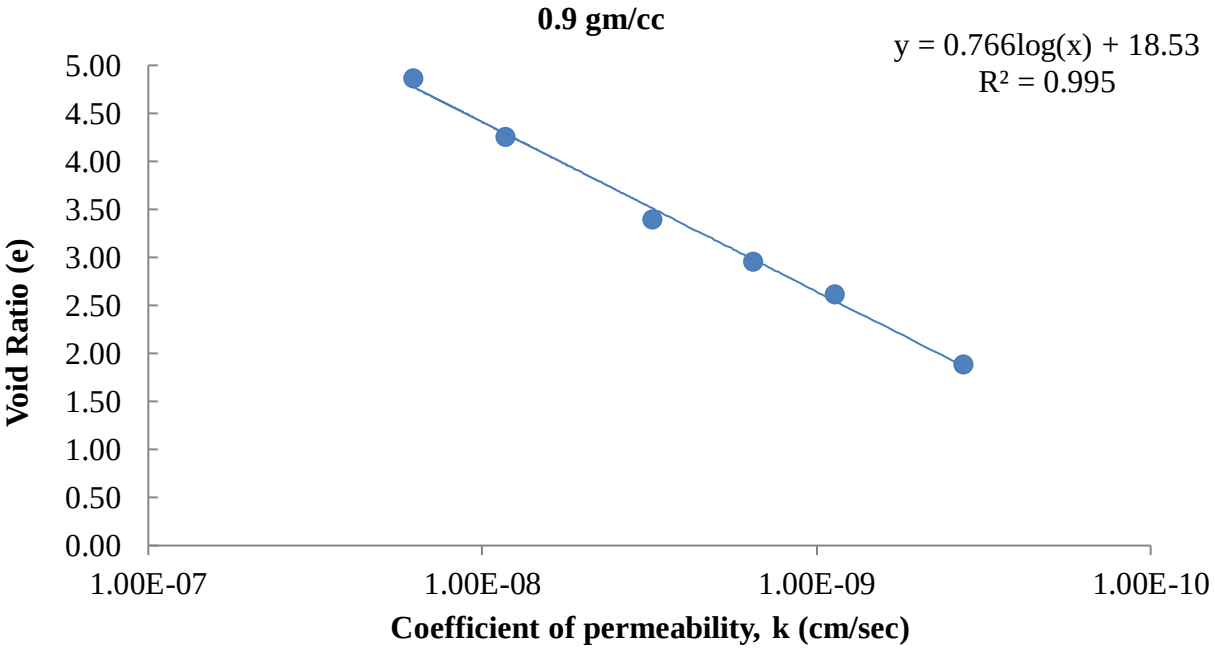

Figure 6.4: e vs log k of density 0.9 gm/cc

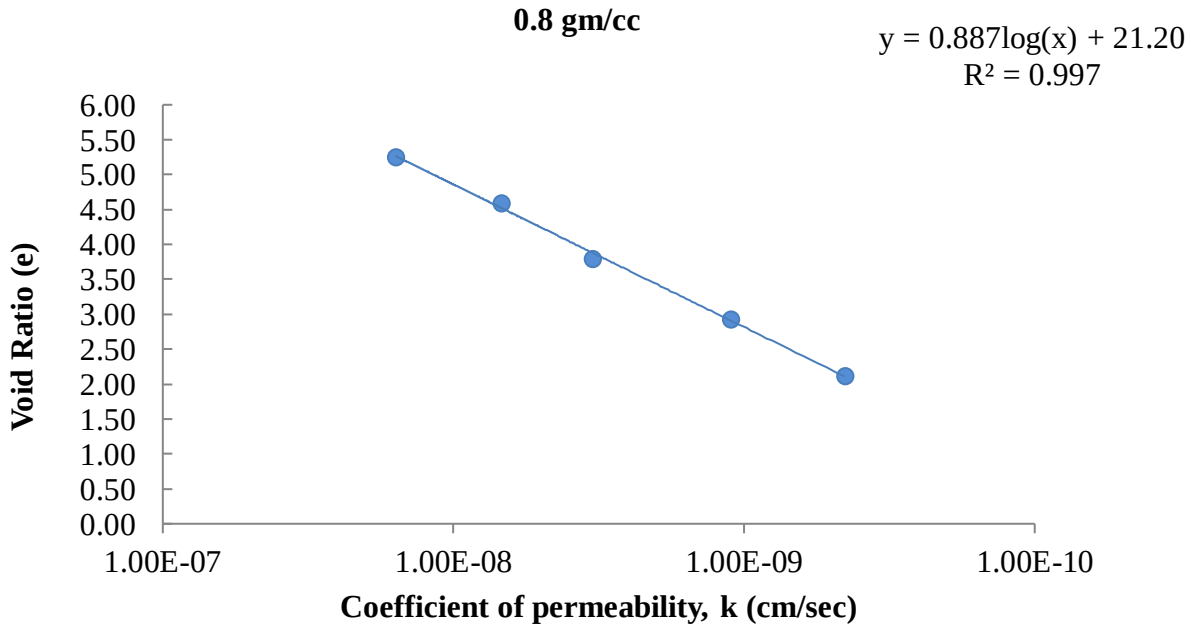

Figure 6.5: e vs log k of density 0.8 gm/cc

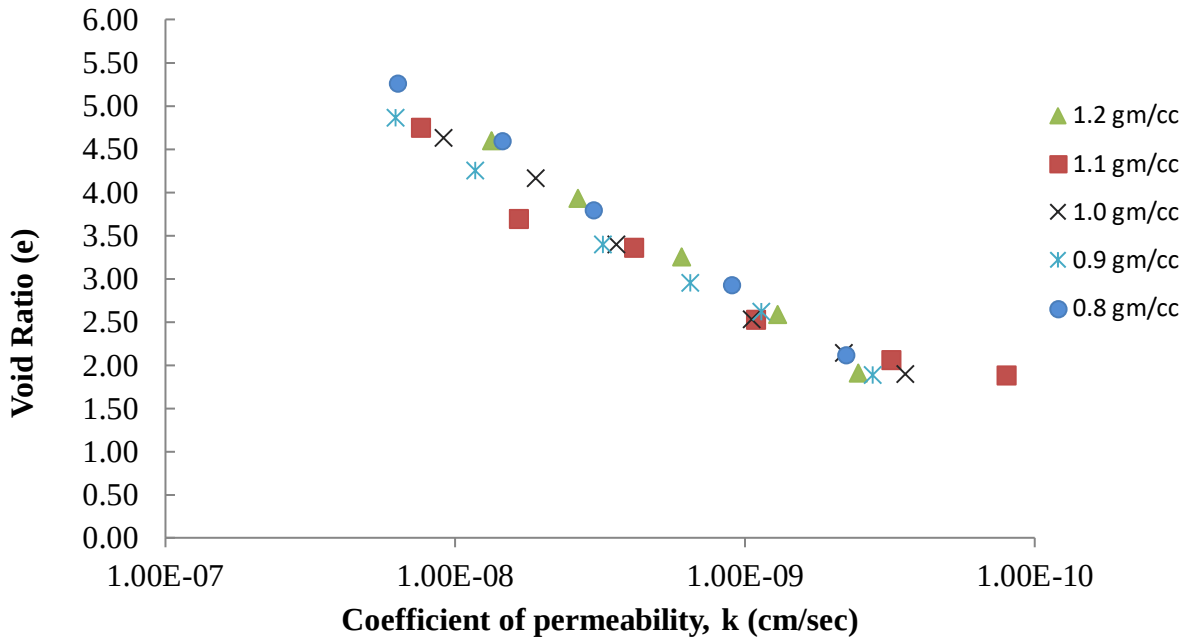

Figure 6.6: Combined graphs of e vs log k

6.3.2 Variation of Permeability with Applied Pressure

The combined data on void ratio versus permeability (Figure 6.6) makes it challenging to directly observe the impact of applied pressure on permeability at different densities. Figures 6.7 to 6.11 provide a detailed visualization of how applied pressure affects permeability across various densities.

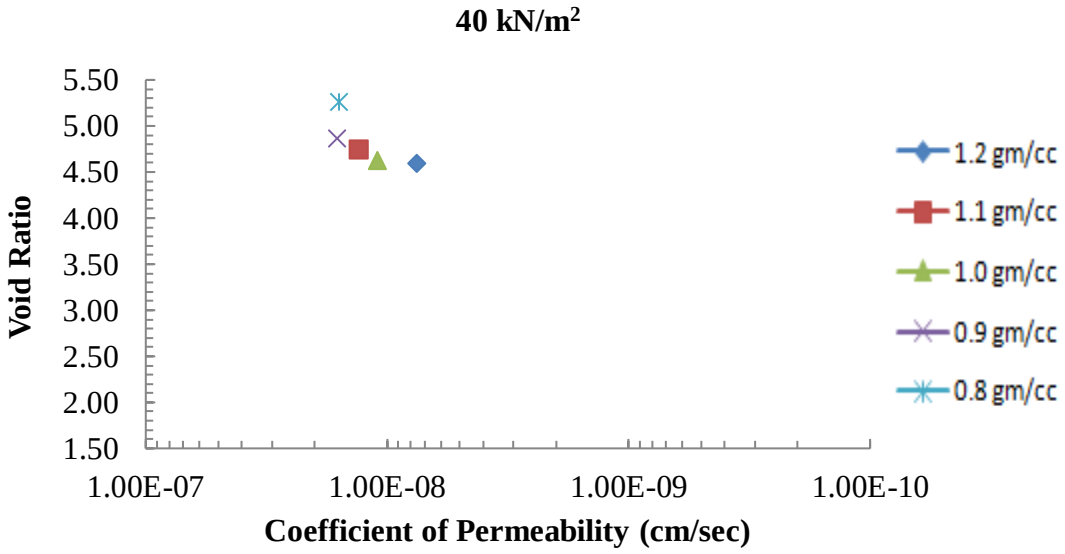

Figure 6.7: e vs log k at 40kN/m^2

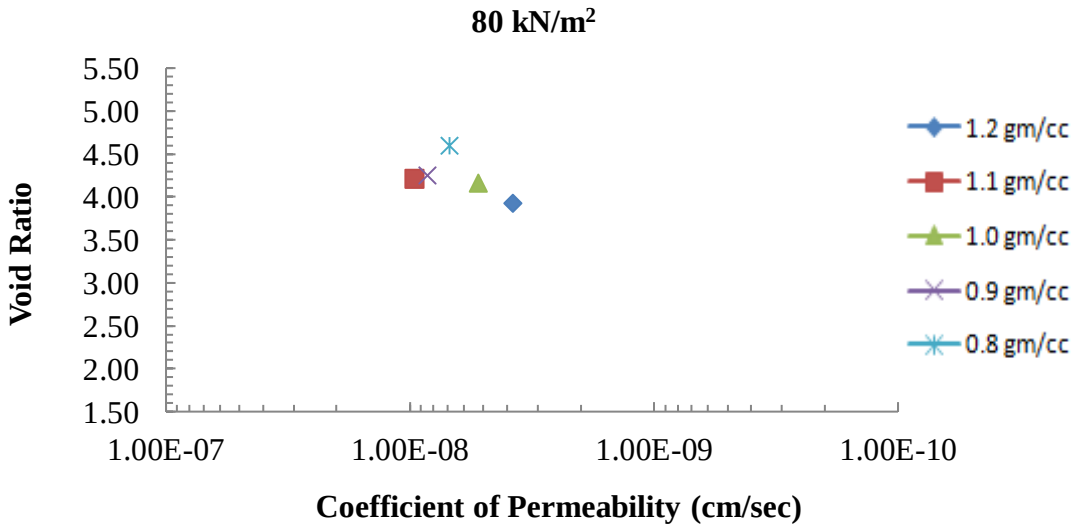

Figure 6.8: e vs log k at 80kN/m^2

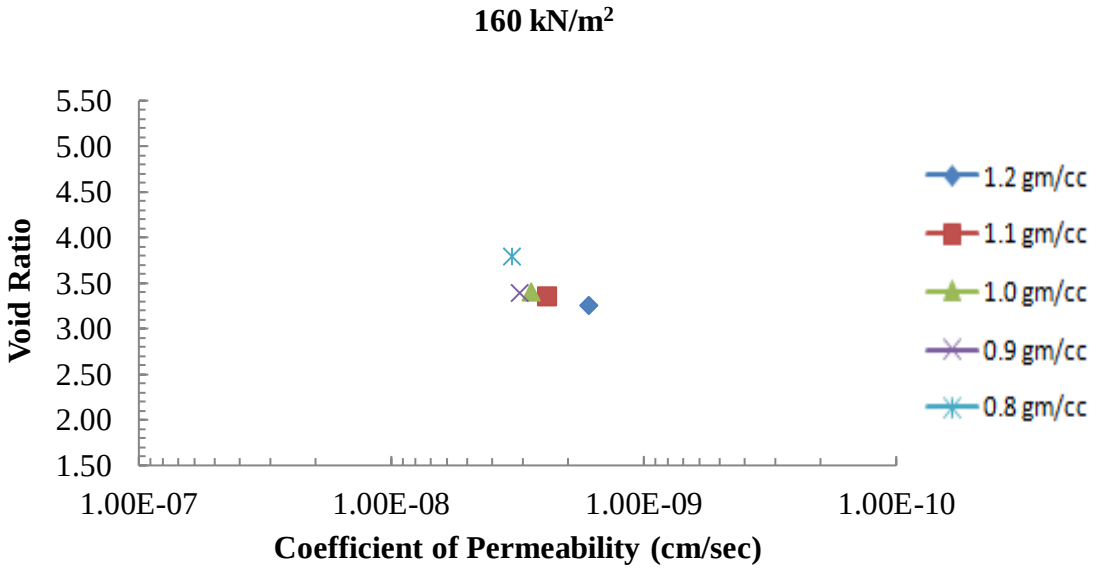

Figure 6.9: e vs log k at 160kN/m^2

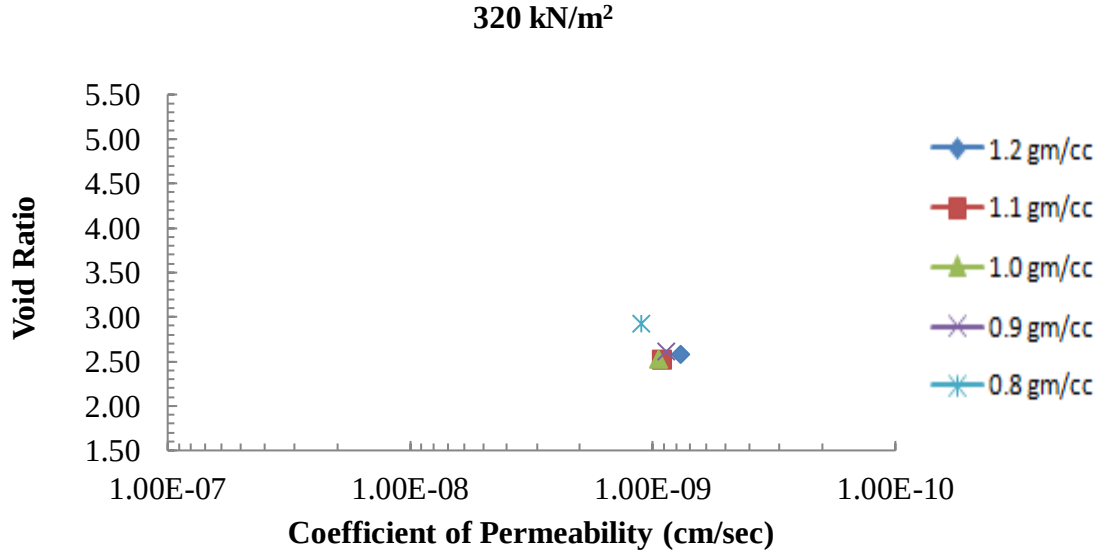

Figure 6.10: e vs log k at 320kN/m^2

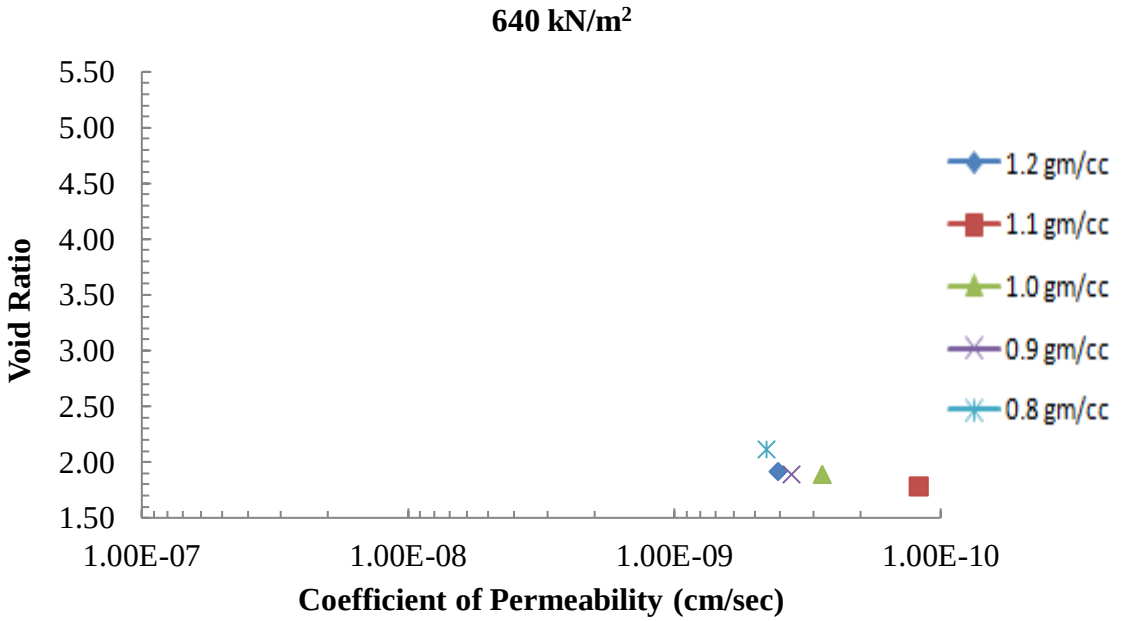

Figure 6.11: e vs log k at 640kN/m^2

The experimental result shows that the permeability of granulated bentonite exhibits a logarithmic decline with a reduction in void ratio. This trend underscores the significant reduction in the material's ability to transmit water as void spaces are minimized. The permeability of samples compacted at different densities—ranging from 1.2 gm/cc to 0.8 gm/cc was observed to fall within the range of 10^{-8} cm/s to10^{-10} cm/s.

Higher-density samples (e.g., 1.2 gm/cc and 1.1 gm/cc) consistently demonstrated lower permeability values due to tighter particle packing, which restricts the pathways available for water transmission. Conversely, lower-density samples (e.g., 0.8 gm/cc and 0.9 gm/cc) exhibited comparatively higher permeability owing to the presence of greater void spaces.

The application of overburden stress further influences permeability by compressing the samples and reducing void ratios, leading to a corresponding decrease in permeability. This effect is particularly pronounced in samples with initially higher void ratios, as the compressibility of these samples allows for greater reductions in void spaces under stress.

Following saturation, the permeability becomes relatively unaffected by initial density variations. This phenomenon is attributed to the swelling behavior of bentonite, which effectively seals void spaces and creates a uniform barrier to water flow regardless of the initial compaction density.

The plot of permeability under varying effective stress levels further highlights the compressible nature of granulated bentonite. At higher effective stress levels, such as 640 kN/m², the permeability range becomes narrower (1.2×10^{-10} cm/s to 4.5×10^{-10} cm/s). In contrast, at lower stress levels, such as 40 kN/m², the permeability range is broader (1.0×10^{-8} cm/s to 7.5×10^{-9} cm/s). This behavior suggests that increasing stress leads to more uniform permeability values as void spaces are further reduced.

6.4 Prediction of Permeability of Granulated Bentonite

The permeability of granulated bentonite is a key factor in understanding its behavior under varying conditions. To estimate permeability, an empirical correlation was formulated using applied stress, density, and void ratio values derived from consolidation tests. This method offers a reliable approach for predicting the permeability of bentonite, enhancing our understanding of its properties under different stress and density conditions.

Experimental results from consolidation tests conducted on granulated bentonite samples with densities of 1.2, 1.1, 0.9, and 0.8 gm/cc were analyzed. The data, which included applied stress, void ratio, and density, were evaluated using multiple linear regressions. This analysis led to the development of the following empirical correlation.

$$\log_{10} k = -9.83 + 0.434*e - 0.00062*\sigma - 0.136*\text{Density} \quad \ldots(6.2)$$

Where k = Predicted Permeability (cm/sec)

e = Void Ratio

σ = Applied effective stress (kN/m^2)

Density = Density of Granulated bentonite (gm/cc)

Equation (6.2) is applicable to granulated bentonite permeated with distilled water, with a correlation coefficient of R^2=0.95 and a standard error of 0.13.

To evaluate the accuracy of this empirical correlation, permeability data obtained from laboratory experiments on samples with a density of 1.0 gm/cc were compared with predicted permeability values for the same density. These predicted values were calculated using the empirical correlation, enabling a direct comparison between experimental observations and the correlation's predictions. This analysis assesses the reliability and effectiveness of the empirical

correlation in accurately estimating the permeability of granulated bentonite under the tested conditions.

Figure 6.12 shows the plot of the predicted coefficient of permeability versus the observed coefficient of permeability for the 1.0 gm/cc density.

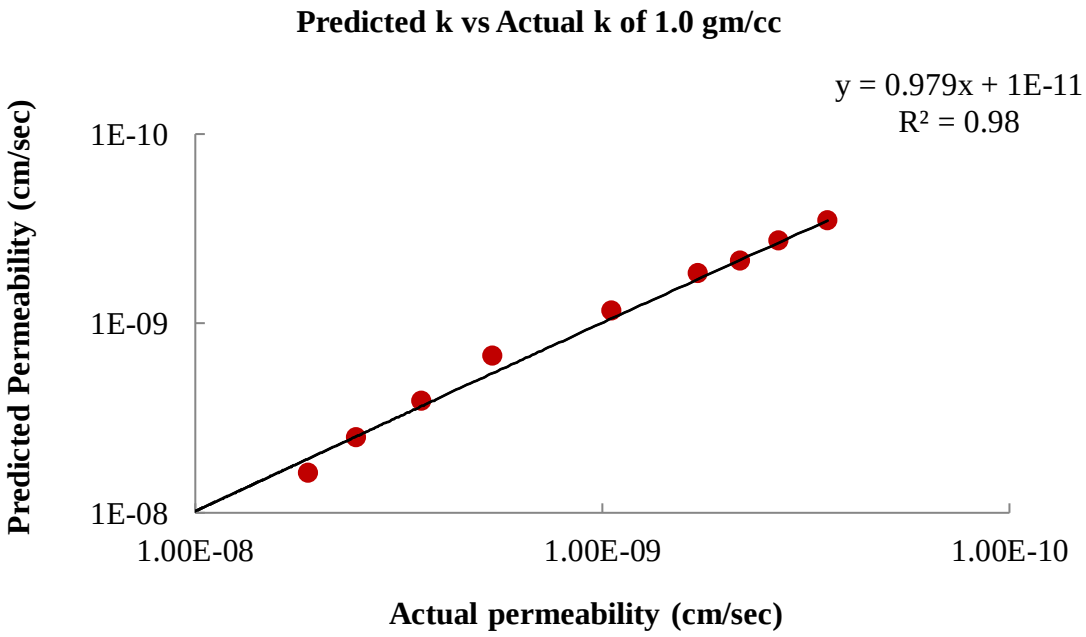

Figure 6.12: Predicted Permeability vs Actual Permeability

Figure 6.12 exhibits an excellent agreement between the predicted and observed permeability values, confirming the reliability of the equation with a correlation coefficient of $R^2 = 0.98$.

CHAPTER 7

CONCLUSION

In this study, the swelling, consolidation, and permeability characteristics of five granulated bentonite samples, compacted at different densities, were examined using a one-dimensional consolidometer with distilled water as the permeating fluid. The research aimed to understand the behavior of granulated bentonite under varying density conditions, focusing on its response to distilled water interaction in terms of swelling potential, consolidation behavior, and permeability.

From this work the following conclusion can be derived:

i. In the oedometric swelling test, the swelling percentage increases with the density of the sample. Additionally, the time required for complete swelling increases with higher density.
ii. Swelling pressure shows a linear increase with density, indicating a direct correlation between compaction and swelling potential.
iii. The compression index decreases with increasing density when distilled water is used as the permeating fluid.
iv. The coefficient of consolidation decreases with both increasing density and effective pressure.
v. The relationship between permeability and density in swelling materials is complex. Higher density initially correlates with lower permeability; however, the swelling process leads to a significant reduction in permeability for all densities. The sealing effect of swelling largely eliminates the influence of initial density on permeability.
vi. A strong correlation was observed between permeability and the density of material, void ratio, and applied stress.

This study has provided valuable insights into the swelling, consolidation, and permeability behavior of granulated bentonite under varying density conditions when it is permeated with distilled water. However, there are several areas where further research could enhance the understanding of this material:

i. Study the behavior of granulated bentonite when permeated with different fluids, such as saline solutions, acidic or alkaline liquids, and industrial effluents.
ii. Evaluate the long-term performance of granulated bentonite under prolonged exposure to water or other fluids.
iii. Investigate the impact of temperature variations on the swelling, consolidation, and permeability properties of granulated bentonite.
iv. Use advanced techniques to examine changes in particle arrangement, pore structure, and mineral interactions during swelling and consolidation.
v. Explore the effects of adding polymers, nanoparticles, or other materials to enhance the engineering properties of granulated bentonite.
vi. Examine the behavior of granulated bentonite with varying mineral compositions and particle sizes to understand the effects of material heterogeneity.

By focusing on these areas, future studies can significantly advance the understanding and practical usability of granulated bentonite in geotechnical and environmental engineering applications.

REFERENCES

1. Alawaji, H.A., (1999), Swell and compressibility characteristics of sand – bentonite mixtures inundated with liquids, *Applied Clay Science*, *15*(3), 411 – 430
2. Baille, W., Tripathy, S. &Schanz, T. (2010). Swelling pressures and one-dimensional compressibility behaviour of bentonite at large pressures. *Applied Clay Science*, *48*, 324–333.http://dx.doi.org/10.1016/j.clay.2010.01.002
3. Cantillo, V., Mercado, V. &Pájaro, C. (2017). Empirical Correlations for the Swelling Pressure of Expansive Clays in the City of Barranquilla, Colombia. *Earth sciences research journal*, *21* (1), 45–49. http://dx.doi.org/10.15446/esrj.v21n1.60226
4. Daniel, D.E. and Wu, Y.K., (1993), Compacted clay liners and covers for arid sites, *Journal of Geotechnical Engineering, ASCE*, *119* (2), 223 – 237.
5. Domitrović, D. &Kovačević B. Z. (2013). The relationship between swelling and shear strength properties of bentonites. *International Conference on Soil Mechanics and Geotechnical Engineering*. 219-222.
6. Herlin, B. &Maubeuge, K.V. (2002). Geosynthetic Clay Liners (GCLs). *4th International Pipeline Conference*, 1-6.
7. Jeon, H. Y. &Lyoo, W.S. (2009). Effects of Additives on Swelling Properties of Modified Bentonites. *GIGSA GeoAfrica 2009 Conference*, 1-8.
8. Liu, L., Neretnieks, I. & Moreno, L. (2011). Permeability and expansibility of natural bentonite MX-80 in distilled water. *Physics and Chemistry of the Earth*, *36*, 1783–1791.
9. Lu, Y., Ye, Wei- Min. & Wang, Q. (2023). Insights into anisotropic swelling pressure of compacted GMZ bentonite. *ActaGeotechnica*, *18* (11), 1-14.
10. Mollins, L.H., Stewart, D.I. & Cousens, T.W. (1996). Predicting the properties of Bentonite- Sand Mixtures. *Clay Minerals*, *31*(2), 243-252.
11. Nagaraj, H. B., Munnas, M. M. & Sridharan, A. (2013). Swelling behavior of expansive soils. *International Journal of Geotechnical Engineering*, *4*, 99-111.
12. Nazir, M., Kawamoto, K., & Sakaki, T. (2021). Properties of granulated bentonite mixtures for radioactive waste disposal: A Review. *International Journal of GEOMATE*, *20* (81), 132-145. https://doi.org/10.21660/2021.81.GX254

13. Punmia, B., Jain, A. K. & Jain, A. K. (2005). *Soil Mechanics and Foundations*. (17th Edition)
14. Pusch, R. (1980). Swelling pressure of highly compacted bentonite. https://inis.iaea.org/collection/NCLCollectionStore/_Public/12/605/12605438.pdf
15. Shirazi, S. M., Kazama, H., Salman, F. A., Othman, F. &Akib, S. (2010). Permeability and swelling characteristics of bentonite. *International Journal of the Physical Sciences*, *5*(11), 1647-1659.
16. Sivapullaiah, P.V., Sridharan, A. & Stalin, V.K. (1996). Swelling behaviour of soil-bentonite mixtures. *Canadian Geotechnical Journal*, *33*(5), 808-814.
17. Sridharan, A., Rao, A.S. & Sivapullaiah, P.V. (1986). Swelling Pressure of Clays. *Geotechnical Testing Journal*, *9*(1), 24-33.
18. Tan, Y., Li, H., Sun, D. & Ming, H. (2020). Granular Bentonite Preparation and Effect of Granulation Behavior on Hydromechanical Properties of Bentonite. *Advances in Civil Engineering*, 1-13.
19. Wang, H. (2024). A device to measure apparent swelling pressure of compacted bentonite using extremely thin specimen.*E3S Web of Conf., 544*. https://doi.org/10.1051/e3sconf/202454401004
20. Watanabe, Y. & Tanaka, Y. (2023). Swelling pressure of compacted bentonite acting on constraining material with deformability. *Géotechnique*, *73* (2), 95–104. https://doi.org/10.1680/jgeot.20.P.348
21. Yong, R.N., Boonsinsuk, P., and Wong, G., (1986), Formulation of backfill material for a nuclear fuel waste disposal vault, *Canadian Geotechnical Journal*, *23*, 216 – 228.
22. Zeng, Z., Cui, Y. J. &Talandier, J. (2022). Effect of water chemistry on the hydro-mechanical behaviour of compacted mixtures of claystone and Na/Ca-bentonites for deep geological repositories. *Journal of Rock Mechanics and Geotechnical Engineering*, *14*, 527-536.
23. Zeng, Z., Cui, Y. J. & Talandier, J. (2023). Evaluation of swelling pressure of bentonite/claystone mixtures from pore size distribution. *ActaGeotechnica*, *18* (3), 1671-1679. https://enpc.hal.science/hal-04181889v1

Appendix I

Table 5.7: Specimen height and void ratio calculation for sample with density 1.2 gm/cc

Applied Pressure (kN/m^2)	Final Dial Reading (mm)	No. of division (a)	Dial change, $\Delta H = a \times L.C.$ (mm)	Specimen height, $H=H1-\Delta H$ (mm)	Height of voids, $H-H_s$ (mm)	Void ratio, $e= (H-H_s)/H_s$
10	1739	43	0.43	22.39	18.94	5.47
20	1641	98	0.98	21.41	17.96	5.19
40	1433	208	2.08	19.33	15.88	4.59
80	1203	230	2.3	17.03	13.58	3.92
160	971	232	2.32	14.71	11.26	3.25
320	739	232	2.32	12.39	8.94	2.58
640	506	233	2.33	10.06	6.61	1.91

Table 5.8: Specimen height and void ratio calculation for sample with density 1.1 gm/cc

Applied Pressure (kN/m^2)	Final Dial Reading (mm)	No. of division (a)	Dial change, $\Delta H = a \times L.C.$ (mm)	Specimen height, $H=H1-\Delta H$ (mm)	Height of voids, $H-H_s$ (mm)	Void ratio, $e= (H-H_s)/H_s$
10	1727	48	0.48	22.27	18.78	5.38
20	1643	84	0.84	21.43	17.94	5.14
40	1503	140	1.4	20.03	16.54	4.73
120	1133	370	3.7	16.33	12.84	3.67
160	1019	114	1.14	15.19	11.7	3.35
320	727	292	2.92	12.27	8.78	2.51
480	563	164	1.64	10.63	7.14	2.04
560	501	62	0.62	10.01	6.52	1.86

Table 5.9: Specimen height and void ratio calculation for sample with density 1.0 gm/cc

Applied Pressure (kN/m^2)	Final Dial Reading (mm)	No. of division (a)	Dial change, $\Delta H = a \times L.C.$ (mm)	Specimen height, $H=H1-\Delta H$ (mm)	Height of voids, $H-H_s$ (mm)	Void ratio, $e= (H-H_s)/H_s$
10	1465	17	0.17	19.65	16.47	5.18
20	1414	51	0.51	19.14	15.96	5.02
40	1289	125	1.25	17.89	14.71	4.63
80	1141	148	1.48	16.41	13.23	4.16
160	899	242	2.42	13.99	10.81	3.40
320	622	277	2.77	11.22	8.04	2.53
480	500	122	1.22	10	6.82	2.14
640	420	80	0.8	9.2	6.02	1.89

Table 5.10: Specimen height and void ratio calculation for sample with density 0.9 gm/cc

Applied Pressure (kN/m^2)	Final Dial Reading (mm)	No. of division (a)	Dial change, $\Delta H = a \times L.C.$ (mm)	Specimen height, $H=H1-\Delta H$ (mm)	Height of voids, $H-H_s$ (mm)	Void ratio, $e= (H-H_s)/H_s$
10	1370	28	0.28	18.7	15.83	5.51
20	1304	66	0.66	18.04	15.17	5.28
40	1182	122	1.22	16.82	13.95	4.86
80	1007	175	1.75	15.07	12.2	4.25
160	760	247	2.47	12.6	9.73	3.39
240	635	125	1.25	11.35	8.48	2.95
320	537	98	0.98	10.37	7.5	2.61
640	328	209	2.09	8.28	5.41	1.88

Table 10.11: Specimen height and void ratio calculation for sample with density 0.8 gm/cc

Applied Pressure (kN/m^2)	Final Dial Reading (mm)	No. of division (a)	Dial change, $\Delta H = a \times L.C.$ (mm)	Specimen height, $H=H1-\Delta H$ (mm)	Height of voids, $H-H_s$ (mm)	Void ratio, $e= (H-H_s)/H_s$
10	1496	33	0.33	17.96	15.40	6.01
20	1425	71	0.71	17.25	14.69	5.73
40	1302	123	1.23	16.02	13.46	5.25
80	1133	169	1.69	14.33	11.77	4.59
160	927	206	2.06	12.27	9.71	3.79
320	706	221	2.21	10.06	7.52	2.92
640	498	208	2.08	7.98	5.42	2.11